eNeuro

Research Article: New Research | Disorders of the Nervous System

MeCP2 Deficiency Leads to Loss of Glial Kir4.1

Uri Kahanovitch[3], Vishnu A. Cuddapah[1], Natasha L. Pacheco[1], Leanne M. Holt[1,3], Daniel K. Mulkey[4], Alan K. Percy[2] and Michelle L. Olsen[1,3]

[1]*Department of Cell, Developmental and Integrative Biology, University of Alabama at Birmingham, Birmingham, Alabama 35294*

[2]*Department of Pediatrics, Civitan International Research Center, University of Alabama at Birmingham, Birmingham, Alabama 35294*

[3]*Virginia Tech School of Neuroscience, Blacksburg, Virginia 24061*

[4]*Department of Physiology and Neurobiology, University of Connecticut, Storrs, Connecticut 06269, USA*

DOI: 10.1523/ENEURO.0194-17.2018

Received: 31 May 2017

Revised: 1 February 2018

Accepted: 8 February 2018

Published: 12 February 2018

Author contributions: U.K., V.A.C., N.L.P., L.H., and M.L.O. performed research; U.K., V.A.C., N.L.P., L.H., and M.L.O. analyzed data; U.K., V.A.C., N.L.P., L.H., D.K.M., and M.L.O. wrote the paper; V.A.C., N.L.P., and M.L.O. designed research; A.P. contributed unpublished reagents/analytic tools.

Funding: http://doi.org/10.13039/100001819—International Rett Syndrome Foundation (IRSF): 2916

Funding: http://doi.org/10.13039/100000002—HHS | National Institutes of Health (NIH): RO1 NSO75062; RO1 HL104101

Funding: UAB CCTS: 5UL1RR025777

Funding: http://doi.org/10.13039/100006464—Civitan International

Funding: http://doi.org/10.13039/100000011—Howard Hughes Medical Institute (HHMI)

The authors declare no competing financial interests.

This work was supported by International Rett Syndrome Foundation for Basic Research Grant (#2916) to MLO, National Institutes of Health grants NS075062 (MLO) and HL104101 (MLO, DKM), the UAB CCTS (grant number 5UL1RR025777) for a pilot grant to MLO, and the Civitan International Research Center for funding to VAC. NLP was funded in part by a grant to the University of Alabama at Birmingham from the Howard Hughes Medical Institute through the Med into Grad Initiative. Additional funds were also provided by Connecticut Department of Public Health Grant 150263 (DKM).

U.K., V.A.C. and N.L.P. authors contributed equally to this work.

Corresponding author: Michelle Olsen, PhD, School of Neuroscience, Life Sciences Building RM 213, 970 Washington St. SW, Blacksburg VA, 24061. Tel: 540-231-7394; E-mail: molsen1@vt.edu

Cite as: eNeuro 2018; 10.1523/ENEURO.0194-17.2018

Title: MeCP2 deficiency leads to loss of glial Kir4.1

Abbreviated title: Kir4.1 is a target of MeCP2

Author names and affiliation, including postal codes

Uri Kahanovitch[3]*, Vishnu A. Cuddapah[1]*, Natasha L. Pacheco[1]*, Leanne M. Holt[1,3], Daniel K. Mulkey[4], Alan K. Percy[2], and Michelle L. Olsen[1,3]

[1]Department of Cell, Developmental and Integrative Biology, University of Alabama at Birmingham, Birmingham, Alabama 35294

[2]Department of Pediatrics, Civitan International Research Center, University of Alabama at Birmingham, Birmingham, Alabama 35294

[3]Virginia Tech School of Neuroscience, Blacksburg, Virginia 24061

[4]Department of Physiology and Neurobiology, University of Connecticut, Storrs, Connecticut USA 06269

*These authors contributed equally

Corresponding author with complete address, including an email address and postal code

Corresponding author:

Michelle Olsen, PhD
School of Neuroscience
Life Sciences Building RM 213
970 Washington St. SW
Blacksburg VA, 24061
P: 540-231-7394
molsen1@vt.edu

Number of figures, tables, multimedia (separately)

Number of Figures: 7

Number of tables: 2

Number of words for abstract, introduction, and discussion (separately)

Number of words for abstract: 235

Number of words for introduction: 541

Number of words for discussion: 1561

Acknowledgements

The authors thank Lucas Pozzo-Miller, PhD and Wei Li, PhD for animals.

Conflicts of Interest

The authors declare no competing financial interests.

Funding sources

This work was supported by International Rett Syndrome Foundation for Basic Research Grant (#2916) to MLO, National Institutes of Health grants NS075062 (MLO) and HL104101 (MLO, DKM), the UAB CCTS (grant number 5UL1RR025777) for a pilot grant to MLO, and the Civitan International Research Center for funding to VAC. NLP was funded in part by a grant to the University of Alabama at Birmingham from the Howard Hughes Medical Institute through the Med into Grad Initiative. Additional funds were also provided by Connecticut Department of Public Health Grant 150263 (DKM).

Abstract

Rett Syndrome (RTT) is an X-linked neurodevelopmental disorder usually caused by mutations in Methyl-CpG-binding protein 2 (MeCP2). RTT is typified by apparently normal development until 6-18 months of age, when motor and communicative skills regress and hand stereotypies, autonomic symptoms, and seizures present. Restoration of MeCP2 function selectively to astrocytes reversed several deficits in a murine model of RTT, but the mechanism of this rescue is unknown. Astrocytes carry out many essential functions required for normal brain functioning including extracellular K^+ buffering. Kir4.1, an inwardly rectifying K^+ channel, is largely responsible for the channel-mediated K^+ regulation by astrocytes. Loss of function mutations in Kir4.1 in human patients results in a severe neurodevelopmental disorder termed EAST or SESAME syndrome. Here we evaluated astrocytic Kir4.1 expression in a murine model of Rett syndrome. We demonstrate by ChIP analysis that Kir4.1 is a direct molecular target of MeCP2. Astrocytes from *Mecp2*-deficient mice express significantly less Kir4.1 mRNA and protein, which translates into a >50% deficiency in Ba^{2+}-sensitive Kir4.1-mediated currents, and impaired extracellular potassium dynamics. By examining astrocytes in isolation we demonstrate that loss of Kir4.1 is cell-autonomous. Assessment through postnatal development revealed that Kir4.1 expression in *Mecp2*-deficient animals never reaches adult, wild-type levels, consistent with a neurodevelopmental disorder. These are the first data implicating a direct MeCP2 molecular target in astrocytes and provide novel mechanistic insight explaining a potential mechanism by which astrocytic dysfunction may contribute to RTT.

Visual Abstract

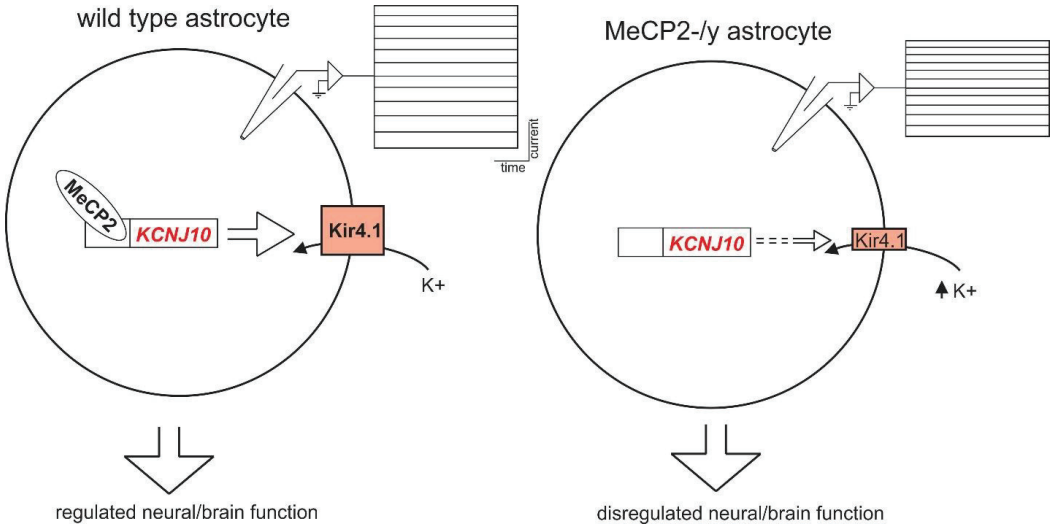

Significance Statement

Rett Syndrome (RTT) is a devastating neurodevelopmental disorder that affects 1 in 10,000-25,000 females. Mutations in Methyl-CpG-binding protein 2 (MeCP2), a transcriptional regulator, are responsible for over 95% of Rett cases. Recent work has shown that astrocytes contribute significantly to the disorder, although their contribution to this disease is not known. Here we demonstrate that the critical astrocyte K^+ channel Kir4.1 is a novel molecular target of MeCP2. MeCP2 deficiency leads to decreased *Kcnj10*/Kir4.1 mRNA levels, protein expression, and currents. These findings provide novel mechanistic insight and begin to elucidate the role of astrocytes in this disorder.

Introduction

Rett Syndrome (RTT) is an X-linked neurodevelopmental disorder that affects 1 in 10,000-25,000 females (Percy, 2002). RTT is characterized by apparently normal development until 6-18 months of age, when deficits in speech, ambulation, and hand use (e.g. hand wringing, clapping) become apparent (Neul et al., 2010). Breathing disturbances, scoliosis, diminished pain response, and seizures are also commonly associated with RTT (Jian et al., 2007; Glaze et al., 2010; Neul et al., 2010). More than 95% of girls with

RTT have a mutation in the Methyl-CpG-binding protein 2 (*MECP2*) gene located on the X-chromosome (Cuddapah et al., 2014). Knockout or mutation of *Mecp2* in mice recapitulates symptoms associated with RTT (Chen et al., 2001; Guy et al., 2001). Functionally, MeCP2 is a methyl-CpG binding-protein, which binds methylated and unmethylated DNA to modulate gene activity, and can act as a repressor or an activator of gene transcription depending on the context (Chahrour et al., 2008).

MeCP2 is most highly expressed in neurons, but it is also expressed in glia cells (Ballas et al., 2009; Kifayathullah et al., 2010; Zachariah et al., 2012; Liu et al., 2015; Liu et al., 2017). In addition, there are indications that astrocytic dysfunction plays a role in the pathophysiology of RTT. RTT astrocytes are abnormal (Maezawa et al., 2009) with altered microtubule assembly (Nectoux et al., 2012) and glutamate clearance (Okabe et al., 2012). Also, when cultured with MeCP2-deficient glia, WT neurons display aberrant morphology (Ballas et al., 2009; Williams et al., 2014). Specific deletion of MeCP2 in astrocytes also resulted in disturbed breathing patterns (Garg et al., 2015). Importantly, postnatal re-expression of MeCP2 in astrocytes in globally *Mecp2*-deficient mice improved locomotion, decreased anxiety, increased lifespan, and normalized respiration, neuronal cell size, and dendritic morphology (Lioy et al., 2011). However, to date, few direct molecular links between astrocytes and astrocytic dysfunction in animal models of Rett syndrome have been demonstrated. Possibly shedding some light on this question, a recent transcriptomic study in MeCP2-deficient mice indicates 46 genes that are unique to astrocytes are disrupted in Rett, one being *Kcnj10*, the gene that codes for Kir4.1, (Pacheco et al., 2017).

Kcnj10 expression is in the top 1% of all expressed genes in astrocytes (Zheng et al., 2014). Underscoring the relative importance of this channel, knockout or mutation of *KCNJ10* causes seizures, ataxia, and developmental deficits in mice and humans alike (Djukic et al., 2007; Bockenhauer et al., 2009; Scholl et al., 2009). Direct evidence that loss of Kir4.1 alters neuronal function was recently demonstrated in a

mouse model of Huntington's disease, where AAV-mediated restoration of Kir4.1 expression specifically to astrocytes reduced the concentration of extracellular K^+ ($[K^+]_o$), prolonged survival, and ameliorated motor abnormalities observed in these mice (Tong et al., 2014). Furthermore, a compound heterozygous change (2 missense mutations) in *KCNJ10* was reported in a patient with Rett-like symptoms that lacked a mutation in *MECP2* (Sajan et al., 2017).

In the current study, we demonstrate Kir4.1 is a direct molecular target of MeCP2. *In situ*, astrocytes from *Mecp2*-deficient mice show smaller astrocytic K^+ currents, with concomitant significant reductions in Kir4.1 protein and transcription. These data suggest MeCP2 is a positive regulator of *Kcnj10* gene expression through development and potentially provide insight explaining how astrocytic dysfunction may contribute to RTT.

Materials & Methods

Animals

All animal procedures were performed in accordance with the [Author University] animal care committee's regulations. Every effort was made to minimize pain and discomfort. WT males were bred with heterozygous *Mecp2*$^{tm1.1Jae}$ (Jaenisch mutation) female mice, which lack exon 3 in the *Mecp2* gene (Chen et al., 2001). Genotypes of offspring were confirmed by PCR of DNA isolated from tail clips. Mutant male mice (*Mecp2*$^{-/y}$) were used for experimentation after P50 when symptomatic, as demonstrated by hypoactivity and hindlimb clasping upon suspension from tail compared to WT littermates of the same age. Symptomatic mutant female mice (*Mecp2*$^{+/-}$) were used for experimentation at 7-8 months of age and compared to WT female mice of the same age. All animals were on a C57BL/6 background.

Western blotting

Animals were anesthetized with CO_2 and quickly decapitated. Brains were removed and placed in ice-cold phosphate-buffered solution (PBS). Under a binocular microscope, the cerebellum and brainstem were removed, and the cortex was separated from hippocampus and midbrain. Cortex, hippocampus, midbrain, cerebellum, and brainstem were collected. Briefly, tissue was placed in ice-cold homogenization buffer (100 mM Tris, pH 7.5, 1% sodium dodecyl sulfate (SDS) at 50 mg/mL) supplemented with protease and phosphatase inhibitors (Sigma) and sonicated for 10 seconds. Tissue homogenates were centrifuged for 5 min at 12,000g at 4°C. Protein quantification was performed on the supernatant using a DC protein assay kit from Bio-Rad (Hercules, CA). Protein was heated to 60°C for 15 minutes in an equal volume of 2X sample buffer (100 mM Tris, pH 6.8, 10% SDS in Laemmli-SDS, 600 mM β-mercaptoethanol). Equal amounts of protein were loaded into a 4-20% gradient pre-cast SDS gel (Bio-Rad). Gels were transferred at 100V for one hour at room temperature to PDVF membrane (Millipore). Membranes were blocked in blocking buffer (10% dried milk in TBST) for one hour before probing with antibodies. The blots were probed with rabbit anti-Kir4.1 (Alomone, 1:1000 for 1 hour), washed three times in TBST and then probed with an HRP-conjugated secondary (Santa Cruz) for one hour. After three 10 min washes, membranes were developed with Classico chemiluminescent reagent (Millipore) using a Kodak film developing system (Kodak). The blots were then stripped and re-probed for chicken anti-GAPDH (Abcam 1:2000 for 1 hour) or rabbit anti-β-tubulin (Millipore, 1:5000 for 30 minutes), which was used as a loading control. Protein expression was quantified using Image J. Target protein was normalized to GAPDH expression in the same lane. Both tetrameric (~150 kDa) and monomeric (~50 kDa) Kir4.1 isoforms were detected (e.g. Figure 3A) that are specific to Kir4.1 as they are not present in *Kcnj10* knockout animals or in negative control lysates (Olsen et al., 2006). The analysis included the entire lane (both isoforms). Cortical and brainstem western blots were run in triplicate or quadruplicate. Human embryonic kidney cell (HEK) lysates were used as a negative control for astrocytic proteins on western blots. Relative amounts of protein are reported.

Quantitative PCR

mRNA was isolated from either cultured astrocytes or cortical and brainstem tissue collected as above using an RNA isolation kit (Qiagen). mRNA was converted to cDNA using the VILO Superscript kit (Life Technologies). Quantitative real-time PCR was run using TaqMan specific probes (all from Life Sciences) for *Kcnj10* (Kir4.1, Mm00445028_m1), Gfap (GFAP, Mm01253033), Hexb (Hexosaminidase B, Mm01282432_m1), *Tmem119* (Transmembrane protein 119, Mm00525305_m1), *Mbp* (Myelin basic protein, Mm01266402_m1), *Rbfox3* (NeuN, Mm01248771_m1) and *Gapdh* (GAPDH, Mm99999915_g1). All probes span exon boundaries and as such only amplify mRNA. Each sample was run in triplicate and normalized to *Gapdh*, and the comparative Ct method was used to calculate changes in gene expression.

Astrocyte isolation

Astrocyte isolation was performed according to (Holt and Olsen, 2016). Briefly, mice were anesthetized with CO_2 and rapidly decapitated, and their cortices micro-dissected in ice-cold cutting solution (120mM NaCl, 3 mM KCl, 2 mM $MgCl_2$, 0.2 mM $CaCl_2$, 26.2 mM $NaHCO_3$, 11.1 mM glucose, 5 mM HEPES), supplemented with AP5 (3 mM) and CNQX (3 mM) and bubbled with 95% oxygen. The tissue was minced and enzymatically dissociated with Papain Dissociation kit (Worthington) following manufacturer instructions. After dissociation, myelin debris and microglia were removed using Myelin Removal Kit (Miltenyi Biotec) and Cd11b+ Microbeads (Miltenyi Biotec), respectively. Astrocytes were then acutely isolated using Anti-ACSA-2+ (astrocyte cell surface antigen 2) MicroBead kit (Miltenyi Biotec). The ASCA-2+ epitope is from the astrocyte-specific β2 subunit of the sodium potassium exchanger (Batiuk et al., 2017). The anti-ACSA-2+ antibody is highly specific for astrocytes (Holt and Olsen, 2016), is robustly expressed in astrocytes (Kantzer et al., 2017), and is used as a first choice option for isolating astrocytes (Batiuk et al., 2017). Manufacturer instructions were generally followed,

except incubation times were extended to 25 minutes and total volume of microbeads was increased to 20-40 µL.

Primary astrocyte cultures

Astrocytes from RTT or wild type littermates were isolated from postnatal day 3-6 pups as described above. Astrocytes were plated on 13 mm glass coverslips coated with poly-l-ornithine and laminin in 24-well plates at a density of 1.0 x 10^5 cells. Astrocytes were maintained in serum-free media (50% Neurobasal Medium (Thermo Fisher), 50% MEM, 1 mM sodium pyruvate, 2 mM glutamine, and B27). Media was changed every day for the three consecutive days, with subsequent media changes every 3-4 days. RNA was collected after 7 and 14 days in vitro (DIV) using Ambion's PureLink RNA Isolation Kit.

Primary astrocyte culture immunohistochemistry

Astrocytes were fixed for immunofluorescence after 7DIV. Cells were first washed with cold PBS, followed by fixation with 4% paraformaldehyde for 15 minutes at room temperature. Subsequently, cells were incubated for 1 hour in blocking buffer (10% goat serum, 0.3% Triton-X in PBS). Astrocyte processes were stained with overnight incubation with Dako anti-rabbit GFAP (Z0334) at 1:1000 concentration. Fluorescent images were acquired with an Olympus VS-120 system.

Acute brain slice preparation

Mice were anesthetized with CO_2 and rapidly decapitated. Brain was quickly isolated and placed in icy ACSF cutting solution (see above). All solutions were continuously bubbled with 95 % O_2 / 5 % CO_2 to bring to pH 7.4. Coronal 300 µm slices were cut with a Leica VT1000A vibratome and placed in artificial cerebrospinal fluid (ACSF) at room temperature containing the following in mM: 120 NaCl, 3 KCl, 1 $MgCl_2$, 2 $CaCl_2$, 26.2 $NaHCO_3$, 11.1 glucose, and 5 HEPES. Slices were allowed to recover for 45 minutes at room temperature before use.

K^+-sensitive microelectrodes

Borosilicate glass capillary tubes (Warner Instrument Corporation; Cat# GC200F-10; OD: 2.0 mm, ID: 1.16 mm) were washed in concentrated nitric acid, water, then 100 % EtOH, and dried overnight at 200 °C. Pipettes were pulled on Sutter Instrument Model P-97 and then placed upright and incubated above a dish containing silane (bis(dimethylamino)dimethylsilane) for 5 minutes at 200 °C. Using a fine-tipped syringe (MICROFIL 28 AWG, World Precision Instruments), K^+ ion exchanger (IE190, World Precision Instruments) was filled at the pipette tip, with care taken to ensure no bubbles. Pipettes were then back-filled with 100 mM KCl. K^+-sensitive microelectrodes were calibrated with solutions containing (in mM) 133 NaCl, 3 KCl, 1.5 $CaCl_2$, 1.2 NaH_2PO_4, 1 $MgCl_2$, 10 glucose, and 8.55 HEPES or 106 NaCl, 30 KCl, 1.5 $CaCl_2$, 1.2 NaH_2PO_4, 1 $MgCl_2$, 10 glucose, and 8.55 HEPES after every experiment. All experiments were performed using a World Precision Instruments electrometer (model FD 223), digitized with a Digidata 1440A (Molecular Devices), and stored and analyzed using Clampex 10.2. K^+ responses, at depths from 40-75 μm into the slice, in layer II/III of the cortex resulting from 3 consecutive, 1-second stimulations of 100 μA at 20 Hz (0.1 μs pulse width) in layer IV/V of the cortex were recorded. Signals were low-pass filtered at 10 Hz.

Whole-cell patch clamp electrophysiology

Patch pipettes were pulled from thin-walled borosilicate glass (World Precision Instruments, catalog no. TW150F-4) and filled with pipette solution containing the following in mM: 125 K-gluconate, 10 KCl, 10 HEPES (free acid), 10 disodium creatine phosphate, 2 MgATP, 0.2 NaGTP, and 0.5 EGTA. The pipette solution was brought to pH 7.3 with KOH and 285-290 mOsm with sucrose. After filling patch pipettes with pipette solution, final resistances were 6-8 MΩ. Slices were transferred to a Zeiss Examiner D1 equipped with a 40X water-immersion lens and Zeiss Axiocam MRm for imaging and constantly perfused with ~30 °C ACSF. Astrocytes were identified using morphological features. Recordings were made with

an Axopatch 200B amplifier (Molecular Devices), low-pass filtered at 1 kHz, and digitized with Digidata 1440A (Molecular Devices). Data were acquired and stored on a personal computer using Clampex 10.2. Cell capacitance and series resistance were compensated using the amplifier. Cell capacitance was measured from the amplifier. Experiments with a series resistance up to 12 MΩ were used, and series resistance was compensated by 80% to reduce voltage errors. Steady-state currents were measured.

Chromatin immunoprecipitation

Half of a brain from 7-9 week old *Mecp2*$^{+/y}$ and *Mecp2*$^{-/y}$ mice was collected for chromatin immunoprecipitation (ChIP) analysis. Chromatin preparation was performed using the Magna ChIP G Tissue Kit (Millipore) according to manufacturer's instructions. Briefly, samples were sheared in a 1X Tissue Stabilizing Solution (Millipore) with protease inhibitors using a 1 mL pipette tip. Samples were then fixed in 1% formaldehyde for 10 minutes at 37°C with minor agitation. The fixation was quenched using 10X Glycine (for final concentration at 1X) and incubated for 5 minutes at room temperature. Cross-linked samples were washed 3 times in ice-cold 1X PBS with protease inhibitors. Samples were then lysed on ice in Tissue Lysis Buffer with protease inhibitors for 15 minutes, with brief vortexing every 5 minutes. Samples were resuspended in 600 µL of ChIP Dilution Buffer with protease inhibitors and sonicated on wet ice under the following conditions: 10 second pulse, 50 second rest, 20% amplitude, 5 total cycles. After sonication, samples were centrifuged at 15,000 rcf at 4°C for 10 min. The resulting supernatant was collected and distributed into 200 µL aliquots for immunoprecipitation.

The immunoprecipitation (IP), washes, reverse cross-linking, and DNA collection and purification were performed as outlined in (Li et al., 2012) with the following modifications: 1) Additional ChIP Dilution Buffer with protease inhibitors was added to each aliquot for a final volume of 500 µL. 2) Both IPs and inputs were digested using 10 µL 0.5 M EDTA, 20 µL 1 M Tris pH 6.5, and 1 µL 20 mg/mL Proteinase K (Clontech) for 1 hour at 55°C with minor agitation. DNA was collected and purified using the Qiagen PCR Purification kit according to manufacturer instructions with the following modifications:

1) At final elution step, EB buffer was incubated on the column for 10 minutes before centrifugation; 2) Final DNA was eluted in 50 µL. Quantitative PCR (qPCR) was performed on the Bio-Rad CFX96 machine using the Applied Biosystems SYBR Select Master Mix for CFX. qPCR cycling parameters were as follows: 95°C for 3 minutes, followed by 40 cycles of 95°C for 10 seconds, 60°C for 30 seconds, and 72°C for 45 seconds, and a final incubation at 70°C for 10 minutes. Primer efficiency was verified through melt curve analysis (60°C for 1 minute, and 0.5°C increments starting at 60°C up to 95°C for 15 seconds each) and running qPCR products on a 1.5% agarose gel. Primers used to amplify specific regions within *Kcnj10* promoter region are listed in Table 1. The ddCT method was used to determine fold change expression in *Mecp2*$^{+/y}$ relative to *Mecp2*$^{-/y}$ mice. Briefly, the ddCT was calculated as the following:

$$dCT = CT^{IP(MeCP2 \text{ or } IgG)} - (CT^{Input} - 6.644)$$, where 6.644 represents 1% starting input

$$ddCT = dCT(Mecp2^{+/y} \text{ or } Mecp2^{-/y}) - \text{Average MeCP2}^{-/Y}\ dCT$$

Fold change expression was calculated using the formula 2^{-ddCT} for both *Mecp2*$^{+/y}$ and *Mecp2*$^{-/y}$ mice.

Data analysis

Data were organized in Microsoft Excel or Origin 8.5. Unless stated otherwise two-tailed t-tests were performed as appropriate, except for non-normally distributed in which case Mann-Whitney non-parametric test was performed. In Figure 5, a 2-way ANOVA was performed with Tukey post-hoc comparison. The statistical tests were performed using InStat 3 (GraphPad Software, La Jolla, CA) or MYSTAT (SYSTAT Software, San Jose, CA). All data are reported as average ± standard error of the mean.

Results

Kir4.1 currents are significantly decreased in Mecp2$^{-/y}$ *mice*

Astrocytes contribute to symptomology of RTT (Lioy et al., 2011). However, few studies have examined the functional differences between wild type and RTT astrocytes. Kir4.1, a glia-specific inward rectifying channel, is critical for normal CNS function. Mutations in *KCNJ10* have been linked to developmental

disorders characterized by early onset seizures, ataxia, epilepsy, and profound developmental delay (Kofuji et al., 2000). Of note, these symptoms are also observed in Rett syndrome. We therefore sought to investigate the properties of Kir4.1 channel function and expression in Rett syndrome.

MeCP2 expression is high in cortical tissue and apparent cortical dysfunction is observed in *Mecp2*-deficient mice (Kishi and Macklis, 2004; D'Cruz et al., 2010). Kir4.1 currents were measured in layer I and layer II/III cortical astrocytes of symptomatic *Mecp2* mutant male (*Mecp2*$^{-/y}$) mice and littermate age and sex- matched controls. To isolate Kir4.1 currents, we stepped cortical astrocytes from a holding potential of -80 mV to 0 mV, and then from -180 to 100 mV in 20 mV increments. We then washed on 100 µM $BaCl_2$, a concentration that specifically blocks Kir channels (Ransom and Sontheimer, 1995), and subtracted out currents that were sensitive to $BaCl_2$. As there were no significant difference between astrocytes in layer I and layer II/III (data not shown), we pooled both layers together. Astrocyte recordings obtained from WT mice (n=24) displayed large-amplitude, linear currents typical of passive astrocytes (Zhou et al., 2006). As depicted in Figure 1E, the 'passive' Ba^{2+}-sensitive Kir4.1 currents were smaller in *Mecp2*$^{-/y}$ astrocytes (n=19). While whole-cell currents were significantly smaller in *Mecp2*$^{-/y}$ astrocytes (Figure 1C), which could be partially explained by smaller Ba^{2+}-sensitive Kir4.1 currents, there was also a decrease in other unidentified Ba^{2+}-insensitive currents in *Mecp2*$^{-/y}$ astrocytes (Figure 1D). In an attempt to identify other K^+ channels disrupted in the cortex of MeCP2-deficient mice, we mined RNA sequencing data from a recent transcriptomic study performed in the cortex of WT and symptomatic MeCP2-deficient mice which were age matched with the current study. Of the 15 *Kcnj* genes identified in this RNA sequencing study, only Kcnj10 (Kir4.1) and Kcnj16 (Kir5.1, a channel thought to form heteromers with Kir4.1, but not form homomeric channels) were significantly downregulated in the cortex of MeCP2 deficient mice (Table 2). Of the 14 *Kcnk* genes identified, only Kcnk2 (Trek-1) was differentially expressed and it was modestly upregulated. Together, these data suggest that a loss of

Kir4.1 homomers and possibly Kir4.1/Kir5.1 heteromeric channels contribute to the reduced K^+ conductance observed in MeCP2 deficient mice.

Kir4.1 channels contribute to the intrinsic membrane properties of astrocytes (Kofuji et al., 2000; D'Ambrosio et al., 2002; Neusch et al., 2006; Olsen et al., 2006; Djukic et al., 2007; Chever et al., 2010; Ma et al., 2014). Therefore, we examined input resistance and resting membrane potential (RMP) in WT and *Mecp2*$^{-/y}$ cortical astrocytes. Kir4.1 has a high open probability at rest (reviewed in Nwaobi et al., 2016) and the relative expression levels of Kir4.1 correlate with the astrocyte input resistance. Lower Kir4.1 channel activity in *Mecp2*$^{-/y}$ mice was associated with a significantly higher membrane resistance (Figure 1B; 15.9 ± 2.8 MΩ in WT vs. 33.2 ± 5.6 MΩ in *Mecp2*$^{-/y}$; p=0.006; n=19-23). However, both genotypes showed similar hyperpolarized resting membrane potential (-77.9 ± 0.7 mV in WT vs. -76.6 ± 0.9 mV in *Mecp2*$^{-/y}$; p=0.23; n =19-24) and whole-cell capacitance, a measure of cell size (18.5 ± 1.5 pF in WT versus 20.3 ± 2.9 pF in *Mecp2*$^{-/y}$; p=0.56; n=19-24). The lack of a change in RMP is in contrast to previous reports regarding the importance of Kir4.1 to the RMP of astrocytes (Olsen et al., 2006; Djukic et al., 2007; Seifert et al., 2009). The lack of a change in resting membrane potential in Rett astrocytes may be explained by the partial reduction in current in *Mecp2*$^{-/y}$ mice as opposed to complete knock-out (Kir4.1 KO mice) or knockdown (siRNA knock down in cultured astrocytes) as published in previous reports. Astrocytes are thought to be selectively permeable to K^+ ions, as such, the remaining Kir4.1 and leak channels would maintain the resting membrane potential near the K^+ equilibrium potential. Alternatively, the increased *Kcnk2* gene expression in the cortex of MeCP2$^{-/y}$ mice may compensate for lower levels of Kir4.1 expression.

$[K^+]_o$ homeostasis is dysregulated in MeCP2$^{-/y}$ mice

Given the previously demonstrated role of astrocytes in the buffering and maintenance of $[K^+]_o$ (Kofuji and Newman, 2004), we assessed whether K^+ homeostasis is disrupted in *Mecp2*$^{-/y}$ mice. To test this, we

stimulated neuronal activity in layer IV/V of the cortex with a 1 second stimulus (20 Hz, 100 μA) followed by a 30 second recovery, performed 3 times in series. Changes in $[K^+]_o$ were measured in layer II/III with a calibrated K^+-sensitive microelectrode. Upon insertion of the K^+-sensitive microelectrode into the slice, we detected a spike in $[K^+]_o$ followed by a fall to a steady-state level. Consistent with the possibly that MeCP2 regulates Kir4.1 expression and consequentially K^+ homeostasis, we found the peak of this K^+ spike to be larger in *Mecp2*$^{-/y}$ mice as compared to WT littermates (5.2 ± 0.5 mM in WT versus 7.9 ± 1.2 in *Mecp2*$^{-/y}$; Figure 2B *left panel*; $p < 0.05$; n = 7-8). Additionally, steady-state $[K^+]_o$ was also higher in *Mecp2*$^{-/y}$ mice as compared to WT littermates (4.2 ± 0.2 mM in WT versus 5.1 ± 0.4 in *Mecp2*$^{-/y}$; Figure 2A dashed line, 2B *middle panel*; $p < 0.05$; n = 7-8). Intriguingly, a similar elevation in baseline K^+ was observed in a murine model of Huntington disease, which showed similar reductions in astrocyte Kir4.1 mediated currents (Tong et al., 2014). We also observed an increase in the amplitude of the K^+ undershoot after the second stimulation (Figure 2A, arrows). The amplitude of the undershoot under baseline increased from 0.03 ± 0.02 mM in WT to 0.08 ± 0.02 mM in MeCP2$^{-/y}$ mice (Figure 2B *right panel*; $p < 0.05$; n = 6-9). Using a similar approach, Chever et al., demonstrated the appearance of a significant undershoot following stimulation in the hippocampus of GFAP-targeted Kir4.1 knock out mice. Together, these data indicate that K^+ homeostasis is disrupted in MeCP2$^{-/y}$ mice and support the possibility that loss of MeCP2 disrupts Kir4.1 function.

Kir4.1 protein expression is significantly downregulated in Mecp2$^{-/y}$ *mice*

To investigate whether decrease in currents stems from decreased Kir4.1 protein expression, we examined Kir4.1 expression in the cortex. We isolated the cortex through micro-dissection and a Western blot analysis revealed 63% downregulation of Kir4.1 protein expression in *Mecp2*$^{-/y}$ mice as compared to littermate controls, with glyceraldehyde 3-phosphate dehydrogenase (GAPDH) and tubulin used as loading controls (Figure 3A, B; $p < 0.05$; n = 10-12). The bands on the Western blot represent both tetrameric (~150 kDa) and monomeric (~50 kDa) isoforms of Kir4.1 (Figure 3A), which are

commonly observed when blotting for Kir4.1 and are not observed in negative control samples (human embryonic kidney cells or in Kir4.1 KO mice (Olsen et al., 2006)). Intriguingly, higher multimers of Kir4.1 are associated with developmental upregulation of the channel that occurs during postnatal development and astrocytic maturation (Dibaj et al., 2007) and these higher molecular weight bands are reduced in MeCP2 deficient mice.

We have recently shown that Kir4.1 is expressed at significantly higher levels in the brainstem relative to other CNS structures (Nwaobi et al., 2014). Therefore, we also examined whole brainstem homogenates from WT and *Mecp2*$^{-/y}$ to determine if Kir4.1 was affected in this structure. Western blots indicate a 20% downregulation of Kir4.1 in the brainstem (Figure 3B; $p < 0.05$; $n = 9$-12). Given that a deficiency of Kir4.1 may also contribute to hyperexcitability in the hippocampus (Calfa et al., 2011b), we probed for Kir4.1 expression and found a 36% downregulation (Figure 3B; $p < 0.05$; $n = 6$-7). Loss of Kir4.1 in cortex, brainstem, and hippocampus may contribute to altered function in these brain regions in *Mecp2*$^{-/y}$ mice.

Kir4.1 is most highly expressed in astrocytes but also expressed in oligodendrocytes and NG2+ glia (Nwaobi et al., 2016). To evaluate Kir4.1 expression in WT and *Mecp2*$^{-/y}$ in astrocytes specifically, as compared to a whole cortical homogenate, magnetic cell separation (MACS) was used (Holt and Olsen, 2016). Astrocytes were isolated from symptomatic MeCP2-deficient males and their age-matched littermates. Western blot analysis from isolated astrocytes in WT and Mecp2-deficient mice indicate Kir4.1 is significantly decreased (Figure 3C, D; $p < 0.01$). The reduction is similar both in whole cortex and isolated astrocytes (Figure 3D).

Kir4.1 (Kcnj10) RNA expression is significantly downregulated in Mecp2$^{-/y}$ *and Mecp2*$^{-/+}$ *mice*

As we demonstrated a global decrease in expression of Kir4.1 protein in *Mecp2*-deficient mice (Figure 3), we next examined if *Kcnj10* transcription is altered in the RTT brain. As a first step, we performed quantitative polymerase chain reaction (qPCR) on micro-dissected samples isolated from symptomatic

356 *Mecp2*$^{-/y}$ mice and WT littermates to examine *Kcnj10* gene expression. In all brain regions, there was a
357 significant loss of *Kcnj10* transcription (Figure 4A): midbrain (41 ± 15%, $p<0.05$) cerebellum (32 ± 3%,
358 $p<0.001$), brainstem (31 ± 5%, $p<0.001$), cortex (31 ± 5%, $p<0.001$) and hippocampus (18 ± 8%, $p<0.05$).
359 Additionally, MACS-isolated astrocytes from P60 symptomatic *Mecp2*$^{-/y}$ mice cortex also showed
360 reduction in *Kcnj10* transcription, same as in the whole brain (Figure 4B, 33 ± 25% $p<0.05$).

361 Most research involving murine models of RTT involve mutant male mice, although RTT typically affects
362 females. Female mice present a slightly less severe and more heterogeneous symptomology that has a
363 delayed onset, due to variable X-chromosome inactivation (Calfa et al., 2011a). The mutation in our
364 mice, the Jaenisch mutation, expresses in half of the neurons, except at 9 month old females in the
365 dentate gyrus which tend to express less (about 40%) the chromosome with the mutation (Smrt et al.,
366 2011). Nonetheless, there is no data concerning the effect of X-linked inactivation in glial cells.
367 However, because RTT typically affects females, we asked if loss of MeCP2 function is also associated
368 with decreased *Kcnj10* mRNA expression in *Mecp2*$^{+/-}$ mice. Symptomatic *Mecp2*$^{+/-}$ mice (7-8 months of
369 age), which displayed motor abnormalities including hind limb clasping, were utilized for these studies.
370 We observed a significant decrease in *Kcnj10* gene expression in *Mecp2*$^{+/-}$ symptomatic females in the
371 cortex (Figure 4C, 1.01 ± 0.08 WT vs. 0.61 ± 0.07 *Mecp2*$^{+/-}$) and brainstem (Figure 4D, 1.01 ± .07 WT vs.
372 0.67 ± 0.11 MeCP2$^{+/}$). Interestingly, the decrease in mRNA in female *Mecp2*$^{+/-}$ mice was significantly
373 larger than that seen in males, although females presumably maintain ~50% MeCP2 expression. The
374 decrease in *Kcnj10* mRNA expression suggests a transcriptional mechanism of regulation.

375 *MeCP2 regulates Kcnj10 transcription in a cell autonomous mechanism*

376 The question remains whether MeCP2 control *Kcnj10* expression via a cell autonomous mechanism (i.e.
377 direct effect of MeCP2 in astrocytes) or via an indirect effect. To attempt to discern between the two
378 possibilities, we used neuronal-free primary cultured astrocytes. Cortical astrocyte from either WT or

379 *Mecp2*$^{-/y}$ P3 mice pups (n=8-12 samples, with 4-6 total cultures, 2 biological replicates per culture) were
380 isolated using the MACS astrocyte isolation as described previously. These astrocytes were cultured for
381 either 7 or 14 days *in vitro* (DIV), when cells were collected and RNA transcription was measured using
382 qPCR. The cultured astrocytes retained their shaped as assessed from GFAP staining (Figure 5A), and the
383 RNA expression profile fitted that of isolated astrocytes: *Gfap* and *Kcnj10* expression matching whole
384 cortex expression, while markers for other cell types were depleted (Figure 5B). We observed no
385 difference in *Kcnj10* transcription between the two genotypes at 7 DIV (Figure 5, p=0.98), when *Kcnj10*
386 transcription levels in situ are also relatively low. In contrast, *Kcnj10* transcription increases significantly
387 in WT astrocytes after 14 DIV, indicative of normal developmental upregulation (Figure 5, p<0.001).
388 Transcription in *Mecp2*$^{-/y}$ astrocytes did not increase (p=0.99) and was significantly reduced when
389 compared to WT astrocytes (p<0.01). These data suggest loss of *Kcnj10* transcription is autonomous to
390 the mutant astrocyte and results from loss of astrocytic *MeCP2*.

391 *Kir4.1 is a direct molecular target of MeCP2*

392 Previous work has demonstrated *Kcnj10* gene expression is robustly, developmentally up-regulated and
393 dependent on the degree of methylation at its promoter (Nwaobi et al., 2014). We postulated that
394 decreased *Kcnj10* transcription might be due to a loss of interaction between MeCP2 and the *Kcnj10*
395 gene in *Mecp2*-deficient mice. To test this, we performed a chromatin immunoprecipitation (ChIP)
396 assay. MeCP2 binds DNA in cytosine-phosphodiester-guanine (CpG) islands that are either methylated or
397 unmethylated to modulate gene expression (Chahrour et al., 2008). To determine if the entire *Kcnj10*
398 gene contained CpG islands, we performed an *in silico* analysis of mouse *Kcnj10* gene (Figure 6A). Two
399 CpG islands were identified: the first spanned the promoter region and the 5' UTR, and the second
400 spanned the transcriptional start site and the initial segment of the exonic region. Because MeCP2 is
401 often bound to actively transcribed promoters (Yasui et al., 2007), we designed four (100-150 bp)
402 overlapping primers to amplify the promoter of *Kcnj10* (Table 1). The ChIP analysis was performed by

probing for a MeCP2 protein interaction with regions 1-4 in the *Kcnj10* promoter. For these experiments, IgG served as a negative control, and RNA polymerase II (RNA Pol II) served as a positive control. Results from these experiments show significant interactions between MeCP2 and sites 1, 2, and 4 of *Kcnj10* in WT mice (Figure 6B). To confirm the specificity of the immunoprecipitation, we performed the ChIP assay with *Mecp2*$^{-/y}$, and did not detect any amplification (Figure 6C). These data are the first demonstrating a direct molecular interaction between MeCP2 and an astrocyte gene target, providing possible mechanistic support for the loss of *Kcnj10* mRNA and its subsequent protein product in *Mecp2*-deficient mice.

Kir4.1 gene and protein expression is downregulated early in disease progression in MeCP2$^{-/y}$ *mice*

Kir4.1 protein levels are markedly increased during early postnatal development, correlating with increased gene transcription and reduced methylation levels of the *Kcnj10* gene (Nwaobi et al., 2014). The most significant increases in gene and protein expression occur from the second through fourth postnatal weeks (Nwaobi et al., 2014) when astrocytes undergo significant morphological refinement and maturation (Bushong et al., 2004). To determine if MeCP2 deficiency altered normal developmental patterns of *Kcnj10* gene expression, we performed qPCR at two developmental time points (P10 and P21), which are early in the disease progression in RTT mice. No difference in *Kcnj10* transcription was observed at P10 (Figure 7A), but we observed a roughly 30% decrease in transcription in the *Mecp2*$^{-/y}$ mice by P21 (Figure 7B; $p < 0.05$; $n = 6$). Western blot analysis indicates a significant deficit in Kir4.1 protein levels in the *Mecp2*$^{-/y}$ (Figure 7C, D; $p < 0.05$; $n = 6$) at both time points. These data demonstrate that normal protein levels of Kir4.1 are not achieved at any time point in *Mecp2*-deficient animals, which may be the result of a direct positive interaction between MeCP2 protein and *Kcnj10* gene promoter that is absent in MeCP2$^{-/y}$ mice.

Discussion

Several recent reports have implicated a role of glia in the progression of RTT (Ballas et al., 2009; Maezawa and Jin, 2010; Lioy et al., 2011; Derecki et al., 2012). Mechanistically, it was hypothesized that RTT astrocytes inhibited neuronal maturation through release of a molecule that stunted dendritic maturity or through deficient release of pro-growth soluble molecule. Previous *in vitro* work also suggests excess glutamate contributes to abnormal neuronal morphology (Maezawa and Jin, 2010). In the current study, we demonstrate that reduced Kir4.1 channel activity in cortical astrocytes. This decrease in channel activity is associated with significant reductions in Kir4.1 protein and mRNA levels and may result from the loss of a direct positive interaction between the MeCP2 protein and the Kcnj10 gene promoter in MeCP2 knockout mice. Supporting this notion, astrocyte cultures derived from MeCP2$^{-/y}$ mice fail to upregulate Kir4.1 in when compared to cultures derived from WT mice. These results indicate the loss of Kir4.1 is autonomous to the astrocyte and provide a mechanism for failure of Kir4.1 developmental upregulation in Rett mice. These data suggest MeCP2 is a positive regulator of *Kcnj10* gene expression through development and potentially provide insight explaining how astrocytic dysfunction may contribute to RTT.

The role of Kir4.1 in RTT and normal brain

Accumulating evidence indicates that Kir4.1 plays an integral role in the central nervous system. Decreased Kir4.1 currents is associated with various pathologies such as epilepsy, cerebral trauma, cerebral ischemia, cerebral inflammation, Alzheimer's disease, amyotrophic lateral sclerosis and Huntington's disease (Nwaobi et al., 2016). Here, we demonstrate that astrocyte Kir4.1 currents are significantly reduced in symptomatic MeCP2 deficient mice. Of note, the extent to which astrocytes are clamped is uncertain due to the leaky membrane and the complex morphology. Reduction in Kir4.1 function may contribute to neuronal dysfunction. Following firing of an action potential, K^+ is extruded from neurons. Due to the small size of the extracellular space, small fluxes in K^+ can lead to large

449 concentration changes that are sufficient to modulate the efficacy of neuronal transmission (Ransom et
450 al., 2000). Regulation of extracellular potassium ($[K^+]_o$) is the most well recognized function of astrocytes
451 (Kuffler and Potter, 1964; Orkand et al., 1966; Kuffler, 1967; Kofuji and Newman, 2004). Basal $[K^+]_o$ in rat
452 hippocampal slices was increased when Kir channels were blocked with $BaCl_2$ (D'Ambrosio et al., 2002).
453 Loss of Kir4.1, with a similar increase in $[K^+]_o$ was reported in a mouse model of Huntington's disease
454 (Tong et al., 2014), and is associated with medium spiny neuron dysfunction. AAV-mediated rescue of
455 Kir4.1 specifically to astrocytes rescued the elevated K^+, prolonged survival, and ameliorated motor
456 deficits in these mice.

457 Our data demonstrates that loss of Kir4.1 in MeCP2-deficient mice is associated with an increase in $[K^+]_o$
458 and K^+ undershoot (Figure 2). Inhibition of Kir4.1 with 200 µM barium in rat hippocampus led to an
459 elevated $[K^+]_o$ and K^+ undershoot (D'Ambrosio et al. 2002) as in our work. The undershoot under normal
460 condition is explained by a model in which Kir4.1 maintains $[K^+]_o$ by efflux of K^+ from astrocytes to
461 balance excessive K^+ uptake by the ATPase (D'Ambrosio et al. 2002). Thus, loss of Kir4.1 leads to a larger
462 K^+ undershoot and perturbation of $[K^+]_o$.

463 Given the role that Kir channels play in the regulation of K^+ concentration, loss of Kir4.1 in RTT may
464 predict a change in neuronal excitability. There are conflicting reports regarding the excitability levels in
465 the *Mecp2*-mutant brains. Some studies show hyperexcitability in various regions of mutant *Mecp2* mice
466 from the level of the neuron (Zhang et al., 2010; Calfa et al., 2011b) up to the level of the neuronal
467 network (Asaka et al., 2006; Moretti et al., 2006; Zhang et al., 2008; D'Cruz et al., 2010; Calfa et al.,
468 2011b; Colic et al., 2011; McLeod et al., 2013). Other studies have not demonstrated the same
469 hyperexcitability in RTT (Dani et al., 2005; Dani and Nelson, 2009; Wood et al., 2009). These discordant
470 findings may be a result of examination at different stages of disease development. Studies reporting
471 measurements from pre-symptomatic to early symptomatic animals (p14-35) show hypoactivity, while
472 studies demonstrating network hyperexcitability use tissue from older mice, which clearly exhibit

473 symptoms associated with RTT (D'Cruz et al., 2010; Colic et al., 2011). Thus, excitability of cortical
474 neurons may dramatically change during disease progression. Supporting this, measurements of cellular
475 density in cortical layers II/III, IV, V, and VI in *Mecp2*$^{-/y}$ mice demonstrate that no abnormalities are
476 observed at P14, but by P56 changes in all cortical layers are apparent (Kishi and Macklis, 2004). This fits
477 the findings in this study, in which Kir4.1 expression is normal in early development, and thus [K^+]
478 regulation by astrocytes may not be disrupted. Failure to upregulate Kir4.1 expression in astrocytes may
479 contribute to the hyperexcitability in aged, symptomatic animals.

480 Supporting the importance of Kir4.1 in normal brain function, patient populations who carry loss-of-
481 function mutations in the *Kcnj10* gene have been identified. Intriguingly, CNS symptoms in these
482 patients, including early onset seizures, ataxia, profound lower motor extremity weakness, and severe
483 cognitive deficits (Scholl et al., 2009; Sicca et al., 2011) are also commonplace in RTT patients. Of note,
484 *Mecp2*$^{-/y}$ cortex demonstrated a significant reduction in Kir4.1 expression, not a complete loss as would
485 be the case in a *Kcnj10* knockout animal. Though Kir4.1 currents are downregulated in *Mecp2*$^{-/y}$ mice,
486 the resting membrane potential of the astrocytes appear unaltered. This may be due to other
487 compensatory K^+ channel regulation in astrocytes.

488 *Impaired developmental regulation of Kir4.1 in RTT mice*

489 Kir4.1 protein and mRNA expression are strongly developmentally up-regulated in all brain regions, with
490 highest expression observed in caudal brain structures (Nwaobi et al., 2014). Throughout the CNS, the
491 increased expression of Kir4.1 parallels the increase in MeCP2 expression and coincides with the onset
492 of symptoms in RTT. Upregulation of Kir4.1 is directly related to the methylation status of several CpG
493 islands found in the promoter and intronic regions of the gene (Nwaobi et al., 2014). Furthermore, the
494 *Kcnj10* promoter is lowly methylated and highly expressed. Given that MeCP2 is a methyl-binding
495 protein, which is often found bound to transcriptionally active genes with lowly methylated promoters

(Yasui et al., 2007; Chahrour et al., 2008), we speculated that MeCP2 was a positive transcriptional regulator of the Kir4.1 gene. Indeed, loss of MeCP2 leads to decreased Kir4.1 expression. Also, we found direct physical interaction between MeCP2 and a CpG-rich island in the promoter of *Kcnj10* using ChIP assay (Figure 6). The data from the cultured isolated astrocytes (Figure 5) suggests loss of *Kcnj10* mRNA is autonomous to the astrocyte and not dependent on development in the diseased CNS. This is the first example of a glia-specific gene targeted by MeCP2 and suggests MeCP2 positively regulates *Kcnj10* gene transcription.

We demonstrate that Kir4.1 expression does not undergo a typical robust developmental upregulation when MeCP2 is absent. Kir4.1 is not downregulated, but instead never reaches normal levels, suggesting that astrocytic maturation may be altered in the absence of MeCP2. *In vivo*, the loss of Kir4.1 that exists before the onset of severe symptomatology in *Mecp2*-deficient mice indicates that it may contribute to disease progression, and not simply an epiphenomenon of a 'diseased' brain.

The vast majority of individuals with RTT are females, yet most animals studies focus on male *Mecp2* mutants. The reasons for this are: (1) male mice present with earlier symptoms and more severe symptoms, and (2) the loss of MeCP2 expression is less variable in male mice. Because the *Mecp2* gene is on the X chromosome, mutant female mice express one WT copy of *Mecp2*, leading to less severe and later symptoms. Additionally, random X chromosome inactivation may lead to skewed expression of the mutant or WT allele, which can cause variable disease progression. Nevertheless, given that RTT largely affects females, we investigated Kir4.1 mRNA expression in aged symptomatic female animals and show a similar loss of *Kcnj10* transcript as that observed in males.

Kir4.1/Kcnj10 dysregulation in Mecp2$^{-/y}$ mice: from direct interaction to function

Transcriptomic and more recently proteomic studies have begun to shed light on gene and protein disruption in human patients and animal models of Rett syndrome (Colantuoni et al., 2001; Gibson et al.,

2010; Gabel et al., 2015; Lin et al., 2016) (Jordan et al., 2007; Chahrour et al., 2008; Urdinguio et al., 2008; Ben-Shachar et al., 2009; Gabel et al., 2015). While no study has systematically evaluated astrocytes, a recent publication indicates that of 46 of 391 differentially expressed genes, are uniquely astrocytic, including Kir4.1 (Pacheco et al., 2017). The changes in astrocyte gene expression do not indicate a typical reactive gliosis as seen in most neurological diseases, as in Rett tissue many markers associated with reactive gliosis are downregulated. Intriguingly, several disrupted genes are developmentally regulated, possibly indicating alterations in astrocyte maturation in the MeCP2-deficient cortex. While numerous studies have demonstrated MeCP2 has many neuronal targets, including Bdnf, Gabr3, Reln, Sst, Creb1 (reviewed in (Singh et al., 2008)), here we show for the first time that one such critical astrocytic gene, *Kcnj10* is a direct molecular target of MeCP2.

Importantly, we also show the first electrophysiological studies performed in astrocytes which indicate normal membrane currents are affected in a mouse model of Rett syndrome. These data may shed light on the role of astrocytes in Rett syndrome and indicate that astrocytes and Kir4.1 may represent novel therapeutic targets for the treatment of RTT.

References

Asaka Y, Jugloff DGM, Zhang L, Eubanks JH, Fitzsimonds RM (2006) Hippocampal synaptic plasticity is impaired in the Mecp2-null mouse model of Rett syndrome. Neurobiology of Disease 21:217-227.

Ballas N, Lioy DT, Grunseich C, Mandel G (2009) Non-cell autonomous influence of MeCP2-deficient glia on neuronal dendritic morphology. Nat Neurosci 12:311-317.

Batiuk MY, de Vin F, Duque SI, Li C, Saito T, Saido T, Fiers M, Belgard TG, Holt MG (2017) An immunoaffinity-based method for isolating ultrapure adult astrocytes based on ATP1B2 targeting by the ACSA-2 antibody. J Biol Chem 292:8874-8891.

Ben-Shachar S, Chahrour M, Thaller C, Shaw CA, Zoghbi HY (2009) Mouse models of MeCP2 disorders share gene expression changes in the cerebellum and hypothalamus. Hum Mol Genet 18:2431-2442.

Bockenhauer D et al. (2009) Epilepsy, ataxia, sensorineural deafness, tubulopathy, and KCNJ10 mutations. N Engl J Med 360:1960-1970.

Bushong EA, Martone ME, Ellisman MH (2004) Maturation of astrocyte morphology and the establishment of astrocyte domains during postnatal hippocampal development. Int J Dev Neurosci 22:73-86.

Calfa G, Percy AK, Pozzo-Miller L (2011a) Experimental models of Rett syndrome based on Mecp2 dysfunction. Exp Biol Med (Maywood) 236:3-19.

Calfa G, Hablitz JJ, Pozzo-Miller L (2011b) Network hyperexcitability in hippocampal slices from Mecp2 mutant mice revealed by voltage-sensitive dye imaging. J Neurophysiol 105:1768-1784.

Chahrour M, Jung SY, Shaw C, Zhou X, Wong STC, Qin J, Zoghbi HY (2008) MeCP2, a Key Contributor to Neurological Disease, Activates and Represses Transcription. Science 320:1224-1229.

Chen RZ, Akbarian S, Tudor M, Jaenisch R (2001) Deficiency of methyl-CpG binding protein-2 in CNS neurons results in a Rett-like phenotype in mice. Nat Genet 27:327-331.

Chever O, Djukic B, McCarthy KD, Amzica F (2010) Implication of Kir4.1 Channel in Excess Potassium Clearance: An In Vivo Study on Anesthetized Glial-Conditional Kir4.1 Knock-Out Mice. Journal of Neuroscience 30:15769-15777.

Colantuoni C, Jeon OH, Hyder K, Chenchik A, Khimani AH, Narayanan V, Hoffman EP, Kaufmann WE, Naidu S, Pevsner J (2001) Gene Expression Profiling in Postmortem Rett Syndrome Brain: Differential Gene Expression and Patient Classification. Neurobiology of Disease 8:847-865.

Colic S, Wither R, Eubanks JH, Zhang L, Bardakjian BL (2011) EEG analysis for estimation of duration and inter-event intervals of seizure-like events recorded in vivo from mice. Conf Proc IEEE Eng Med Biol Soc 2011:2570-2573.

Cuddapah VA, Pillai RB, Shekar KV, Lane JB, Motil KJ, Skinner SA, Tarquinio DC, Glaze DG, McGwin G, Kaufmann WE, Percy AK, Neul JL, Olsen ML (2014) Methyl-CpG-binding protein 2 (MECP2) mutation type is associated with disease severity in Rett syndrome. J Med Genet 51:152-158.

D'Ambrosio R, Gordon DS, Winn HR (2002) Differential role of KIR channel and Na(+)/K(+)-pump in the regulation of extracellular K(+) in rat hippocampus. J Neurophysiol 87:87-102.

D'Cruz JA, Wu C, Zahid T, El-Hayek Y, Zhang L, Eubanks JH (2010) Alterations of cortical and hippocampal EEG activity in MeCP2-deficient mice. Neurobiol Dis 38:8-16.

Dani VS, Nelson SB (2009) Intact long-term potentiation but reduced connectivity between neocortical layer 5 pyramidal neurons in a mouse model of Rett syndrome. J Neurosci 29:11263-11270.

Dani VS, Chang Q, Maffei A, Turrigiano GG, Jaenisch R, Nelson SB (2005) Reduced cortical activity due to a shift in the balance between excitation and inhibition in a mouse model of Rett syndrome. Proc Natl Acad Sci U S A 102:12560-12565.

Derecki NC, Cronk JC, Lu Z, Xu E, Abbott SB, Guyenet PG, Kipnis J (2012) Wild-type microglia arrest pathology in a mouse model of Rett syndrome. Nature 484:105-109.

Djukic B, Casper KB, Philpot BD, Chin LS, McCarthy KD (2007) Conditional knock-out of Kir4.1 leads to glial membrane depolarization, inhibition of potassium and glutamate uptake, and enhanced short-term synaptic potentiation. J Neurosci 27:11354-11365.

Gabel HW, Kinde B, Stroud H, Gilbert CS, Harmin DA, Kastan NR, Hemberg M, Ebert DH, Greenberg ME (2015) Disruption of DNA-methylation-dependent long gene repression in Rett syndrome. Nature 522:89-93.

Garg SK, Lioy DT, Knopp SJ, Bissonnette JM (2015) Conditional depletion of methyl-CpG-binding protein 2 in astrocytes depresses the hypercapnic ventilatory response in mice. J Appl Physiol (1985) 119:670-676.

584 Gibson JH, Slobedman B, H KN, Williamson SL, Minchenko D, El-Osta A, Stern JL, Christodoulou J (2010) Downstream
585 targets of methyl CpG binding protein 2 and their abnormal expression in the frontal cortex of the human Rett
586 syndrome brain. BMC Neurosci 11:53.
587 Glaze DG, Percy AK, Skinner S, Motil KJ, Neul JL, Barrish JO, Lane JB, Geerts SP, Annese F, Graham J, McNair L, Lee HS
588 (2010) Epilepsy and the natural history of Rett syndrome. Neurology 74:909-912.
589 Guy J, Hendrich B, Holmes M, Martin JE, Bird A (2001) A mouse Mecp2-null mutation causes neurological symptoms
590 that mimic Rett syndrome. Nat Genet 27:322-326.
591 Holt LM, Olsen ML (2016) Novel Applications of Magnetic Cell Sorting to Analyze Cell-Type Specific Gene and Protein
592 Expression in the Central Nervous System. PLoS One 11:e0150290.
593 Jian L, Nagarajan L, de KN, Ravine D, Christodoulou J, Leonard H (2007) Seizures in Rett syndrome: an overview from
594 a one-year calendar study. Eur J Paediatr Neurol 11:310-317.
595 Jordan C, Li HH, Kwan HC, Francke U (2007) Cerebellar gene expression profiles of mouse models for Rett syndrome
596 reveal novel MeCP2 targets. BMC Med Genet 8:36.
597 Kantzer CG, Boutin C, Herzig ID, Wittwer C, Reiss S, Tiveron MC, Drewes J, Rockel TD, Ohlig S, Ninkovic J, Cremer H,
598 Pennartz S, Jungblut M, Bosio A (2017) Anti-ACSA-2 defines a novel monoclonal antibody for prospective isolation of
599 living neonatal and adult astrocytes. Glia 65:990-1004.
600 Kifayathullah LA, Arunachalam JP, Bodda C, Agbemenyah HY, Laccone FA, Mannan AU (2010) MeCP2^{270} Mutant
601 Protein Is Expressed in Astrocytes as well as in Neurons and Localizes in the Nucleus. Cytogenetic and Genome
602 Research 129:290-297.
603 Kishi N, Macklis JD (2004) MECP2 is progressively expressed in post-migratory neurons and is involved in neuronal
604 maturation rather than cell fate decisions. Molecular and Cellular Neuroscience 27:306-321.
605 Kofuji P, Newman EA (2004) Potassium buffering in the central nervous system. Neuroscience 129:1043-1054.
606 Kofuji P, Ceelen P, Zahs KR, Surbeck LW, Lester HA, Newman EA (2000) Genetic Inactivation of an Inwardly Rectifying
607 Potassium Channel (Kir4.1 Subunit) in Mice: Phenotypic Impact in Retina. Journal of Neuroscience 20:5733-5740.
608 Kuffler SW (1967) The Ferrier Lecture: Neuroglial Cells: Physiological Properties and a Potassium Mediated Effect of
609 Neuronal Activity on the Glial Membrane Potential. Proceedings of the Royal Society of London Series B, Biological
610 Sciences 168:1-21.
611 Kuffler SW, Potter DD (1964) GLIA IN THE LEECH CENTRAL NERVOUS SYSTEM: PHYSIOLOGICAL PROPERTIES AND
612 NEURON-GLIA RELATIONSHIP. J Neurophysiol 27:290-320.
613 Li W, Calfa G, Larimore J, Pozzo-Miller L (2012) Activity-dependent BDNF release and TRPC signaling is impaired in
614 hippocampal neurons of Mecp2 mutant mice. Proc Natl Acad Sci U S A 109:17087-17092.
615 Lin P, Nicholls L, Assareh H, Fang Z, Amos TG, Edwards RJ, Assareh AA, Voineagu I (2016) Transcriptome analysis of
616 human brain tissue identifies reduced expression of complement complex C1Q Genes in Rett syndrome. BMC
617 Genomics 17:427.
618 Lioy DT, Garg SK, Monaghan CE, Raber J, Foust KD, Kaspar BK, Hirrlinger PG, Kirchhoff F, Bissonnette JM, Ballas N,
619 Mandel G (2011) A role for glia in the progression of Rett's syndrome. Nature 475:497-500.
620 Liu F, Ni J-J, Sun F-Y (2017) Expression of Phospho-MeCP2s in the Developing Rat Brain and Function of Postnatal
621 MeCP2 in Cerebellar Neural Cell Development. Neuroscience Bulletin 33:1-16.
622 Liu F, Ni J-J, Huang J-J, Kou Z-W, Sun F-Y (2015) VEGF overexpression enhances the accumulation of phospho-S292
623 MeCP2 in reactive astrocytes in the adult rat striatum following cerebral ischemia. Brain Research 1599:32-43.
624 Ma B, Xu G, Wang W, Enyeart JJ, Zhou M (2014) Dual patch voltage clamp study of low membrane resistance
625 astrocytes in situ. Mol Brain 7:18.
626 Maezawa I, Jin LW (2010) Rett Syndrome Microglia Damage Dendrites and Synapses by the Elevated Release of
627 Glutamate. Journal of Neuroscience 30:5346-5356.
628 Maezawa I, Swanberg S, Harvey D, LaSalle JM, Jin LW (2009) Rett Syndrome Astrocytes Are Abnormal and Spread
629 MeCP2 Deficiency through Gap Junctions. Journal of Neuroscience 29:5051-5061.
630 McLeod F, Ganley R, Williams L, Selfridge J, Bird A, Cobb SR (2013) Reduced seizure threshold and altered network
631 oscillatory properties in a mouse model of Rett syndrome. Neuroscience 231:195-205.
632 Moretti P, Levenson JM, Battaglia F, Atkinson R, Teague R, Antalffy B, Armstrong D, Arancio O, Sweatt JD, Zoghbi HY
633 (2006) Learning and Memory and Synaptic Plasticity Are Impaired in a Mouse Model of Rett Syndrome. Journal of
634 Neuroscience 26:319-327.
635 Nectoux J, Florian C, Delepine C, Bahi-Buisson N, Khelfaoui M, Reibel S, Chelly J, Bienvenu T (2012) Altered
636 microtubule dynamics in Mecp2-deficient astrocytes. Journal of neuroscience research 90:990-998.

637 Neul JL, Kaufmann WE, Glaze DG, Christodoulou J, Clarke AJ, Bahi-Buisson N, Leonard H, Bailey ME, Schanen NC,
638 Zappella M, Renieri A, Huppke P, Percy AK (2010) Rett syndrome: revised diagnostic criteria and nomenclature. Ann
639 Neurol 68:944-950.
640 Neusch C, Papadopoulos N, Muller M, Maletzki I, Winter SM, Hirrlinger J, Handschuh M, Bahr M, Richter DW,
641 Kirchhoff F, Hulsmann S (2006) Lack of the Kir4.1 channel subunit abolishes K+ buffering properties of astrocytes in
642 the ventral respiratory group: impact on extracellular K+ regulation. J Neurophysiol 95:1843-1852.
643 Nwaobi SE, Lin E, Peramsetty SR, Olsen ML (2014) DNA methylation functions as a critical regulator of Kir4.1
644 expression during CNS development. Glia 62:411-427.
645 Nwaobi SE, Cuddapah VA, Patterson KC, Randolph AC, Olsen ML (2016) The role of glial-specific Kir4.1 in normal and
646 pathological states of the CNS. Acta Neuropathol.
647 Okabe Y, Takahashi T, Mitsumasu C, Kosai K, Tanaka E, Matsuishi T (2012) Alterations of gene expression and
648 glutamate clearance in astrocytes derived from an MeCP2-null mouse model of Rett syndrome. PLoS One 7:e35354.
649 Olsen ML, Higashimori H, Campbell SL, Hablitz JJ, Sontheimer H (2006) Functional expression of Kir4.1 channels in
650 spinal cord astrocytes. Glia 53:516-528.
651 Orkand RK, Nicholls JG, Kuffler SW (1966) Effect of nerve impulses on the membrane potential of glial cells in the
652 central nervous system of amphibia. J Neurophysiol 29:788-806.
653 Percy AK (2002) Rett syndrome. Current status and new vistas. Neurol Clin 20:1125-1141.
654 Ransom CB, Sontheimer H (1995) Biophysical and pharmacological characterization of inwardly rectifying K+
655 currents in rat spinal cord astrocytes. Journal of Neurophysiology 73:333-346.
656 Ransom CB, Ransom BR, Sontheimer H (2000) Activity-dependent extracellular K+ accumulation in rat optic nerve:
657 the role of glial and axonal Na+ pumps. The Journal of Physiology 522:427-442.
658 Sajan SA, Jhangiani SN, Muzny DM, Gibbs RA, Lupski JR, Glaze DG, Kaufmann WE, Skinner SA, Annese F, Friez MJ,
659 Lane J, Percy AK, Neul JL (2017) Enrichment of mutations in chromatin regulators in people with Rett syndrome
660 lacking mutations in MECP2. Genet Med 19:13-19.
661 Scholl UI, Choi M, Liu T, Ramaekers VT, Hausler MG, Grimmer J, Tobe SW, Farhi A, Nelson-Williams C, Lifton RP
662 (2009) Seizures, sensorineural deafness, ataxia, mental retardation, and electrolyte imbalance (SeSAME syndrome)
663 caused by mutations in KCNJ10. Proc Natl Acad Sci U S A 106:5842-5847.
664 Seifert G, Huttmann K, Binder DK, Hartmann C, Wyczynski A, Neusch C, Steinhauser C (2009) Analysis of Astroglial K+
665 Channel Expression in the Developing Hippocampus Reveals a Predominant Role of the Kir4.1 Subunit. Journal of
666 Neuroscience 29:7474-7488.
667 Sicca F, Imbrici P, D'Adamo MC, Moro F, Bonatti F, Brovedani P, Grottesi A, Guerrini R, Masi G, Santorelli FM, Pessia
668 M (2011) Autism with seizures and intellectual disability: possible causative role of gain-of-function of the inwardly-
669 rectifying K+ channel Kir4.1. Neurobiol Dis 43:239-247.
670 Singh J, Saxena A, Christodoulou J, Ravine D (2008) MECP2 genomic structure and function: insights from ENCODE.
671 Nucleic Acids Res 36:6035-6047.
672 Smrt RD, Pfeiffer RL, Zhao X (2011) Age-dependent expression of MeCP2 in a heterozygous mosaic mouse model.
673 Hum Mol Genet 20:1834-1843.
674 Tong X, Ao Y, Faas GC, Nwaobi SE, Xu J, Haustein MD, Anderson MA, Mody I, Olsen ML, Sofroniew MV, Khakh BS
675 (2014) Astrocyte Kir4.1 ion channel deficits contribute to neuronal dysfunction in Huntington's disease model mice.
676 Nat Neurosci 17:694-703.
677 Urdinguio RG, Lopez-Serra L, Lopez-Nieva P, Alaminos M, Diaz-Uriarte R, Fernandez AF, Esteller M (2008) Mecp2-null
678 mice provide new neuronal targets for Rett syndrome. PLoS One 3:e3669.
679 Williams EC, Zhong X, Mohamed A, Li R, Liu Y, Dong Q, Ananiev GE, Mok JCC, Lin BR, Lu J, Chiao C, Cherney R, Li H,
680 Zhang S-C, Chang Q (2014) Mutant astrocytes differentiated from Rett syndrome patients-specific iPSCs have
681 adverse effects on wild-type neurons. Human Molecular Genetics 23:2968-2980.
682 Wood L, Gray NW, Zhou Z, Greenberg ME, Shepherd GMG (2009) Synaptic Circuit Abnormalities of Motor-Frontal
683 Layer 2/3 Pyramidal Neurons in an RNA Interference Model of Methyl-CpG-Binding Protein 2 Deficiency. Journal of
684 Neuroscience 29:12440-12448.
685 Yasui DH, Peddada S, Bieda MC, Vallero RO, Hogart A, Nagarajan RP, Thatcher KN, Farnham PJ, Lasalle JM (2007)
686 Integrated epigenomic analyses of neuronal MeCP2 reveal a role for long-range interaction with active genes. Proc
687 Natl Acad Sci U S A 104:19416-19421.
688 Zachariah RM, Olson CO, Ezeonwuka C, Rastegar M (2012) Novel MeCP2 isoform-specific antibody reveals the
689 endogenous MeCP2E1 expression in murine brain, primary neurons and astrocytes. PLoS One 7:e49763.

690 Zhang L, He J, Jugloff DG, Eubanks JH (2008) The MeCP2-null mouse hippocampus displays altered basal inhibitory
691 rhythms and is prone to hyperexcitability. Hippocampus 18:294-309.
692 Zhang X, Cui N, Wu Z, Su J, Tadepalli JS, Sekizar S, Jiang C (2010) Intrinsic membrane properties of locus coeruleus
693 neurons in Mecp2-null mice. Am J Physiol Cell Physiol 298:C635-C646.
694 Zheng H, Stornetta RL, Agassandian K, Rinaman L (2014) Glutamatergic phenotype of glucagon-like peptide 1
695 neurons in the caudal nucleus of the solitary tract in rats. Brain Struct Funct.
696 Zhou M, Schools GP, Kimelberg HK (2006) Development of GLAST(+) astrocytes and NG2(+) glia in rat hippocampus
697 CA1: mature astrocytes are electrophysiologically passive. J Neurophysiol 95:134-143.

698

Legends

Figure 1. Ba^{2+}-sensitive Kir4.1 currents are significantly reduced in layer II/III astrocytes of *Mecp2*$^{-/y}$ mice.

(A) Representative traces of pre-Ba^{2+}, post-Ba^{2+}, and Ba^{2+}-sensitive currents in WT and *Mecp2*$^{-/y}$ astrocytes. (B) *Mecp2*$^{-/y}$ astrocytes show higher input resistance than their WT littermates. (C-E) Current-versus-voltage graphs (n=19-24) demonstrate that pre-Ba^{2+}, post-Ba^{2+}, and Ba^{2+}-sensitive currents are significantly reduced in *Mecp2*$^{-/y}$ astrocytes (except at the -80 mV step in the pre-Ba^{2+} currents (C) and the Ba^{2+}-sensitive currents (E). In all, results are consistent with a reduction of Kir4.1 currents in the plasma membrane. Mann-Whitney test was conducted for each voltage step between the two genotypes. **p<0.01

Figure 2. $[K^+]_o$ is elevated and $[K^+]_o$ undershoots after stimulation in MeCP2$^{-/y}$ cortex.

(A) Representative changes in $[K^+]_o$ after 3 successive stimulations in WT and *Mecp2*$^{-/y}$ slices. Baseline $[K^+]_o$ (dashed horizontal line) is elevated in *Mecp2*$^{-/y}$ slices. (B) *left:* Peak $[K^+]_o$ increase after insertion of K^+-sensitive microelectrode into slice is greater in *Mecp2*$^{-/y}$ slices. *Middle:* Steady-state $[K^+]_o$ is elevated in *Mecp2*$^{-/y}$ slices. *Right:* K^+ undershoot after the 2nd stimulation is greater in *Mecp2*$^{-/y}$ slices. *p<0.05

Figure 3. Kir4.1 protein is downregulated in *Mecp2*$^{-/y}$ brains.

(A) Representative Western blot of cortical protein lysates from 5 wild type and 6 symptomatic *Mecp2*$^{-/y}$ males demonstrates a significant loss of Kir4.1 protein expression in cortex (~150 kDa tetramer, 37 kDa monomer) when normalized to a loading control (GAPDH or tubulin). (B) Quantification of Image J analysis normalizing Kir4.1 protein expression to GAPDH in cortex. Similar loss of Kir4.1 immunoreactivity in *Mecp2*-deficient male mice is seen in brainstem and hippocampus. In isolated astrocytes, Kir4.1 expression is lower in *Mecp2*$^{-/y}$ mice compared to WT, as in whole cortex lysate (C, D).

Figure 4. Decreased Kir4.1 transcription in *Mecp2*-deficient mice

(A) *Kcnj10* mRNA is significantly downregulated in micro-dissected cerebellum, midbrain, cortex, hippocampus and brainstem of *Mecp2*$^{-/y}$ mice. Similar reduction is observed in isolated cortical astrocytes from *Mecp2*$^{-/y}$ mice (B). (C-D) *Kcnj10* is significantly downregulated in the cortex and brainstem of *Mecp2*$^{+/-}$ symptomatic female mice. *p<0.05, **p<0.01, ***p<0.001

Figure 5. *Loss of Kcnj10 is autonomous to astrocytes*

Using a magnetic-bead sorting technique, isolated astrocytes were plated and kept in serum-free medium for 7 to 14 days. 4-6 cultures were used, with two biological replicates per culture, a total of 8-12 samples. (A) By 7 days, WT astrocytes attain a stellate morphology as indicated by GFAP staining (B) By 14 days in culture astrocytes, *Gfap* and *Kcnj10* expression is enriched compared to age matched cortex. Cultures express low levels of mRNA for other cell types including microglia (HexB, Tmem119), oligodendrocytes (Mbp) and neurons (Rbfox3), indicating relative purity of the astrocyte cultures. (C) When examining the transcription of Kcnj10, there is a significant effect for both genotype (p<0.001) and DIV (p<0.001). There was no difference at 7 days *in vitro* (DIV) between WT and *Mecp2*$^{-/y}$ astrocytes in transcription of *Kcnj10*. Transcription of *Kcnj10* shows a typical developmental increase in WT astrocytes at 14 DIV, while such an increase was not seen with the *Mecp2*$^{-/y}$ astrocytes. 2-way ANOVA was performed with Tukey post-hoc comparison. *p<0.05, ***p<0.001.

Figure 6. *Kcnj10* is a direct molecular target of MeCP2

(A) A schematic of the mouse *Kcnj10* gene indicating the promoter, 5'UTR, intronic, and exonic region of the gene. The relative locations of primers used to query MeCP2 binding are indicated. (B) ChIP results indicate significant physical interaction between MeCP2 and *Kcnj10* in three sites in the promoter of the *Kcnj10* gene (B, sites 1, 2, and 4, $p < 0.05$, n=5), while no interactions are found in the *Mecp2*-null mice (C). *p<0.05, **p<0.01, # p<0.0005, ## p<0.0001

Figure 7. Kir4.1 is not sufficiently upregulated through development in *Mecp2*-deficient mice.

(A) *Kcnj10* mRNA is not significantly different in the cortex of p10 *Mecp2*$^{-/y}$ mice. (B) *Kcnj10* mRNA is significantly decreased in the cortex of p21 *Mecp2*$^{-/y}$ mice. Representative Western blots and Image J quantification demonstrate loss of Kir4.1 protein expression in cortex in both (C) p10 and (D) p21 mice when normalized to a loading control (GAPDH). * $p<0.05$

751 Table 1. Targeted Kir4.1 CpG Island I (promoter) PCR amplification sites

752

Target name	Forward Primer Sequences	Reverse Primer Sequences
CpG I-1	5'-AGTTTCCCTGCTTTCAATCCTG-3'	5'-CCTGTGGGAACACAGACACA-3'
CpG I-2	5'-GGATGGGAAGAGTTTGACGC-3'	5'-TACGGTGCAAAGTGTGGGAG-3'
CpG I-3	5'-CACACTTTGCACCGTACTGC-3'	5'-GATAGAAGCCGAGCTGGCAA-3'
CpG I-4	5'-GGCCGCCTCACTTTTCTTCT-3'	5'-TGGAGAGATTTGGGCAAGGC-3'

753

754

755

756

757

758

759

760

761

762

763 Table 2. RNA sequencing indicates of 14 *Kcnj* and 15 *Kcnk* potassium channels identified in the cortex of
764 symptomatic MeCP2$^{-/y}$ mice and WT age matched littermates, only *Kcnj10*, *Kcnj16* and *Kcnk2* are
765 differentially expressed (data mined from Pacheco et al., 2017).

Protein	Gene Name	FPKM WT	FPKM TG	Fold Change	q value	Cell type specificity
Kir4.1	Kcnj10	80.991	65.281	-0.311	0.00065	Astrocytes/oligodendrocytes/OPC's
Kir5.1	Kcnj16	14.832	11.353	-0.386	0.00853	Astrocytes/OPC's
TREK-1	Kcnk2	25.299	31.559	0.319	0.03503	Astrocytes/neurons/OPC's

766

767

768

769 **Figure 1**

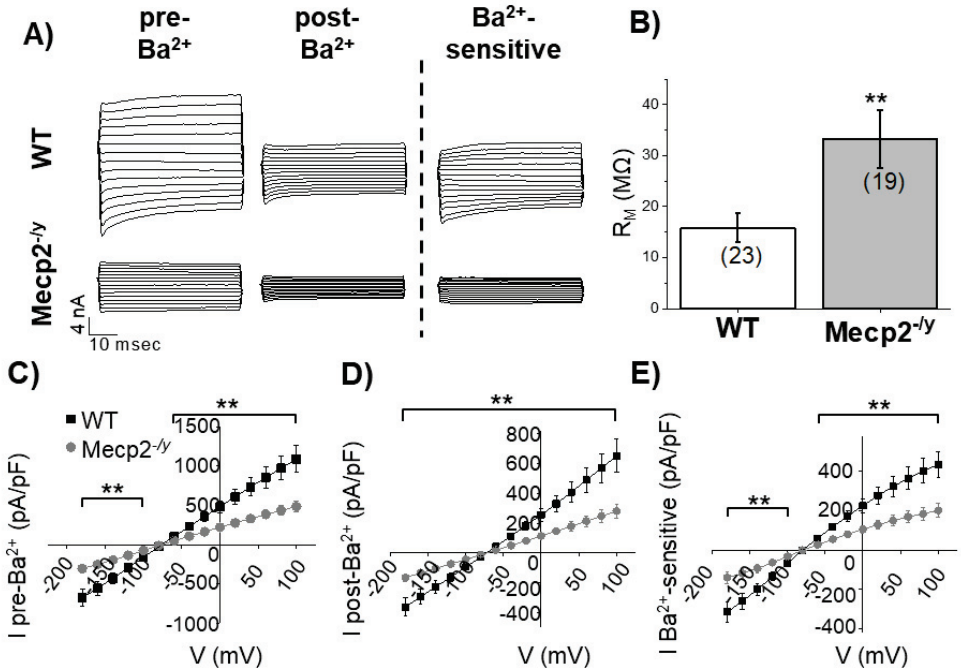

770

771

772 **Figure 2**

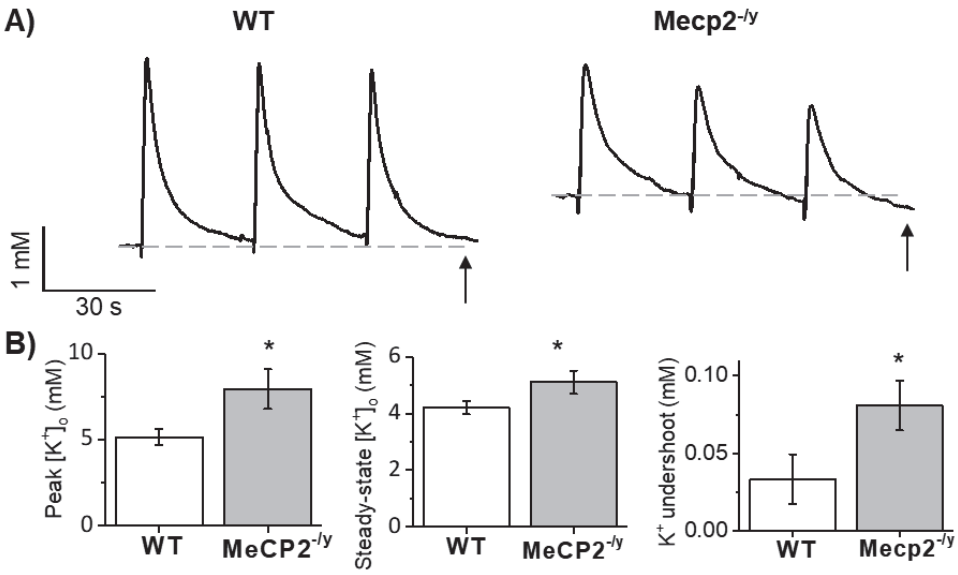

773

774

775 **Figure 3**

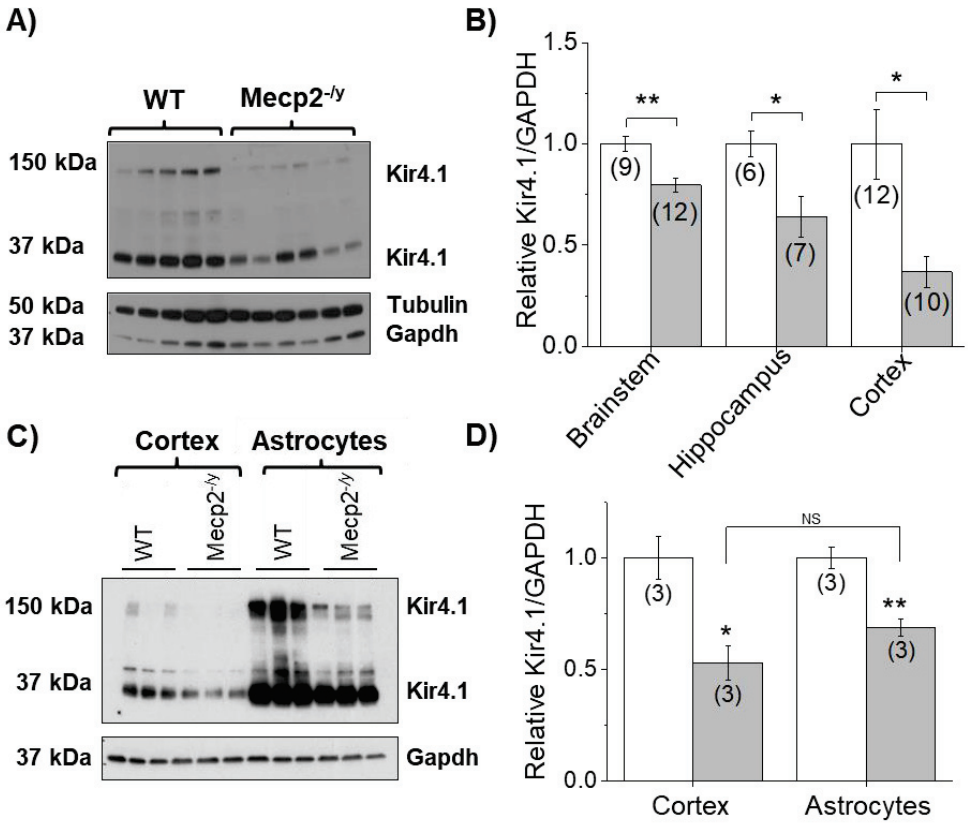

776

777

778 **Figure 4**

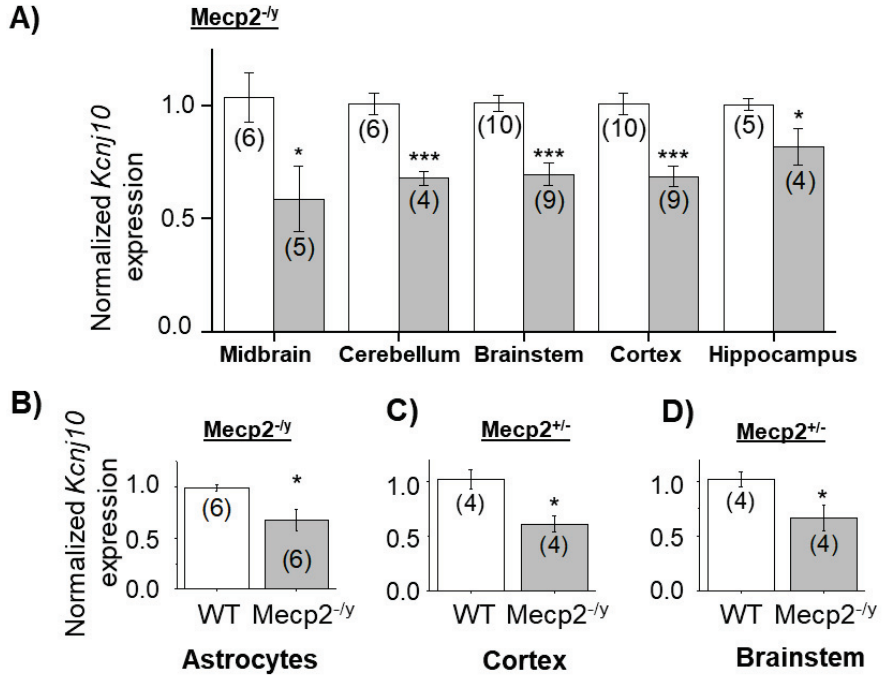

779

780

781 **Figure 5**

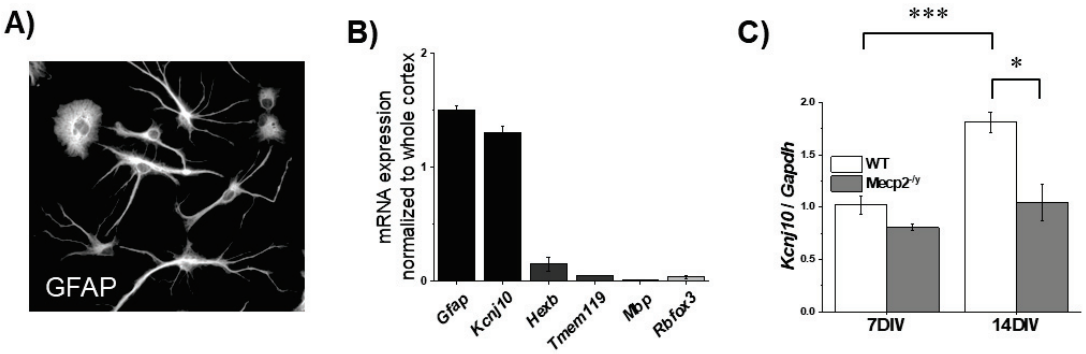

782

783

784 **Figure 6**

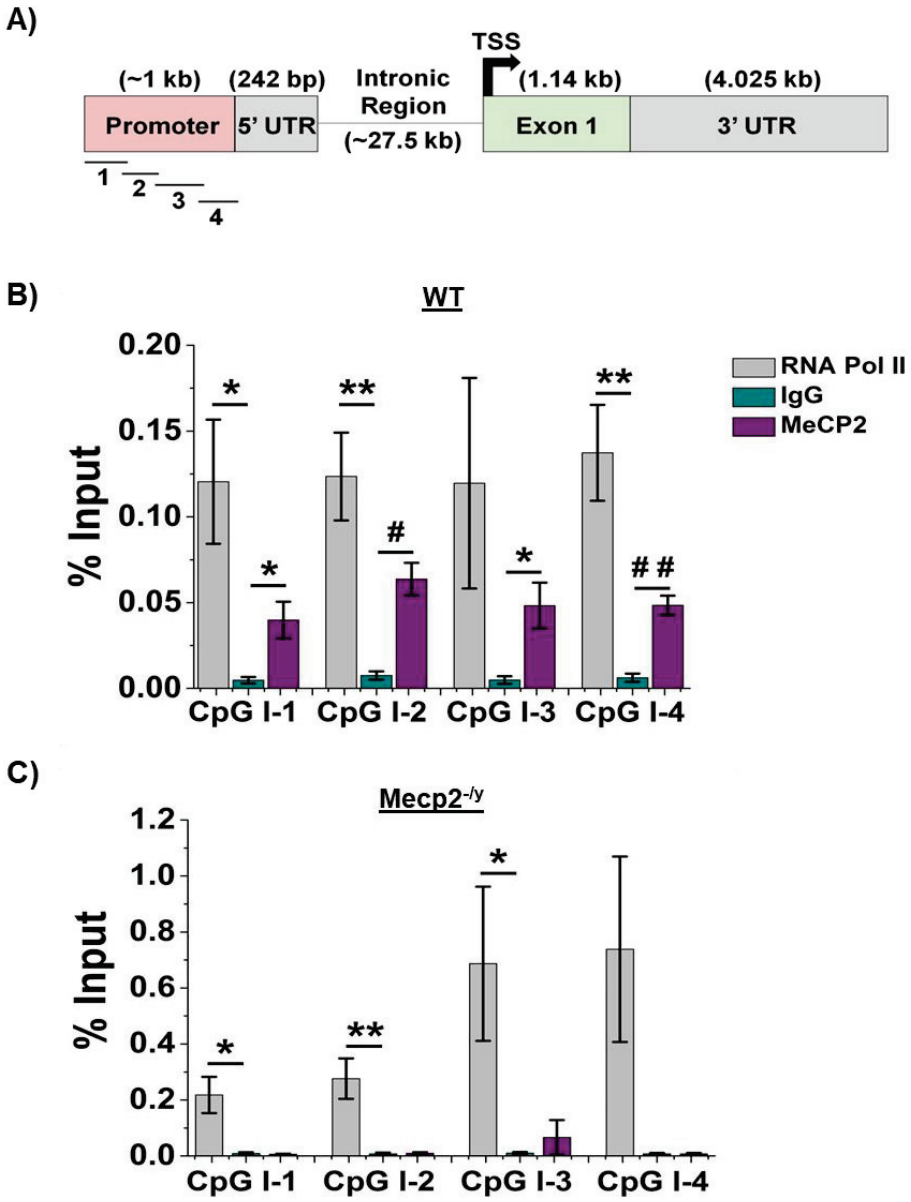

785

786

787 **Figure 7**

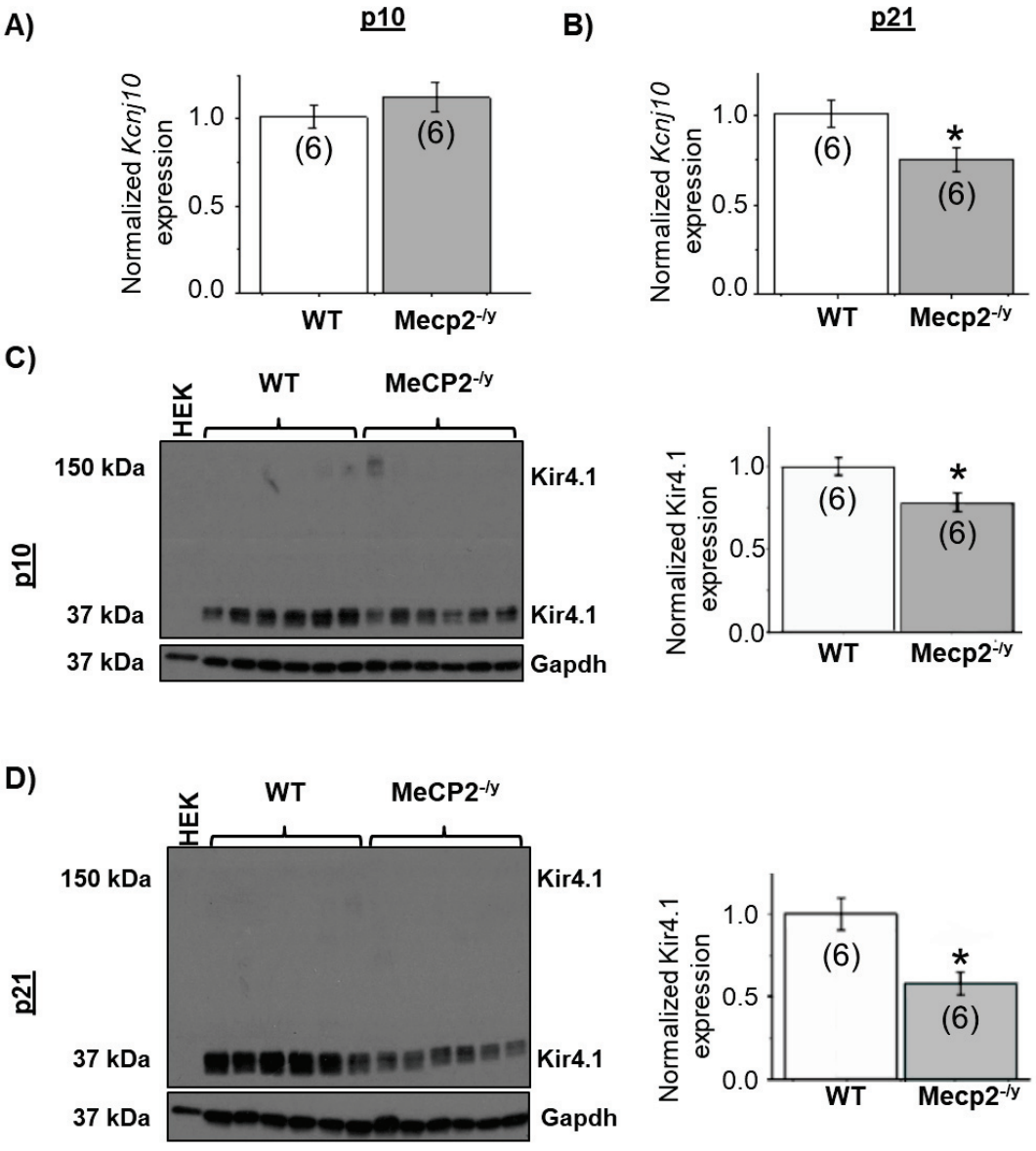

788

789

Figure 1

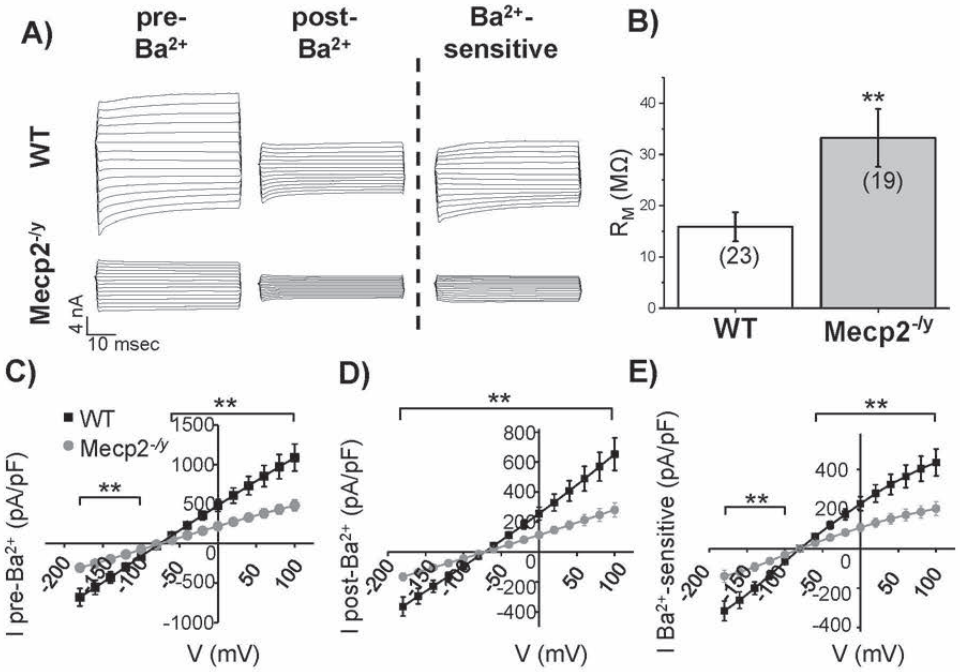

Figure 2

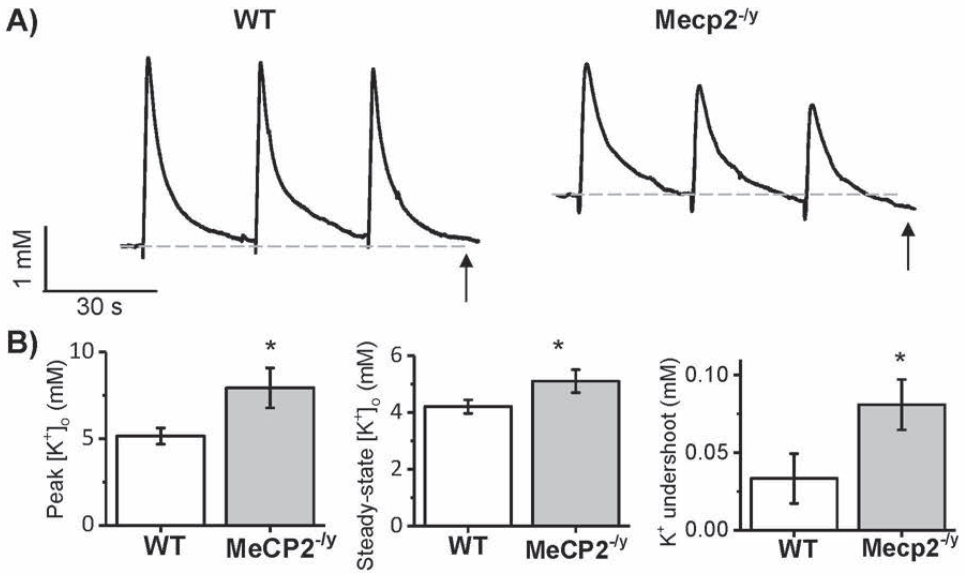

Figure 3

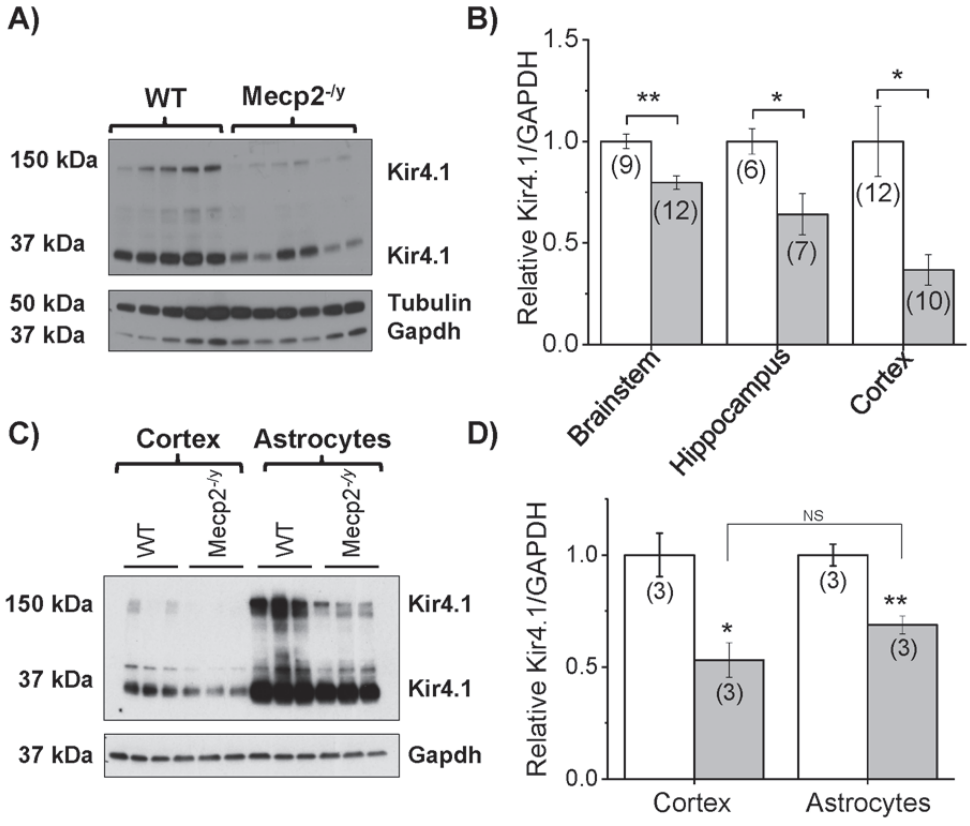

Figure 4

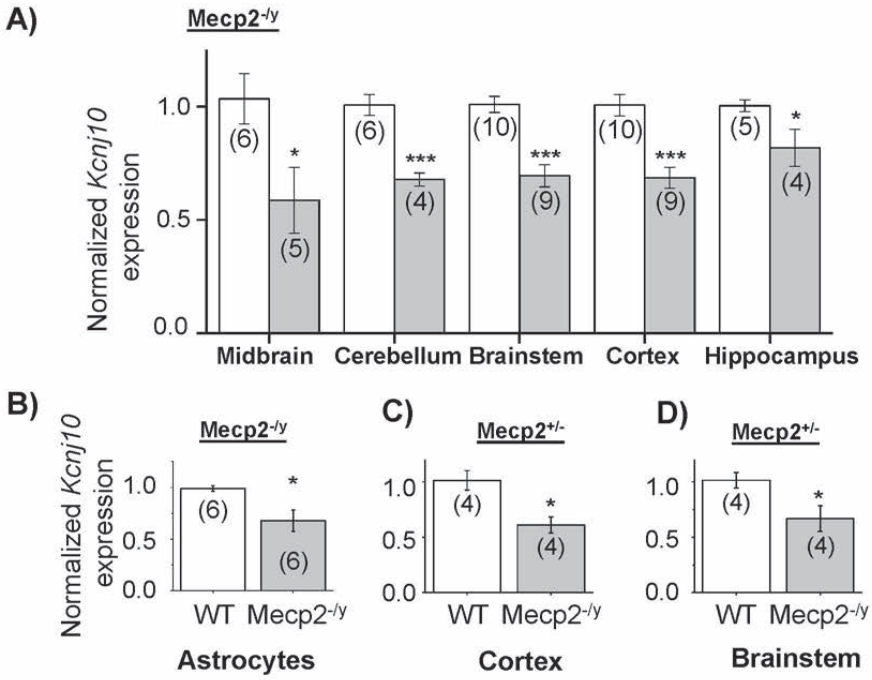

Figure 5

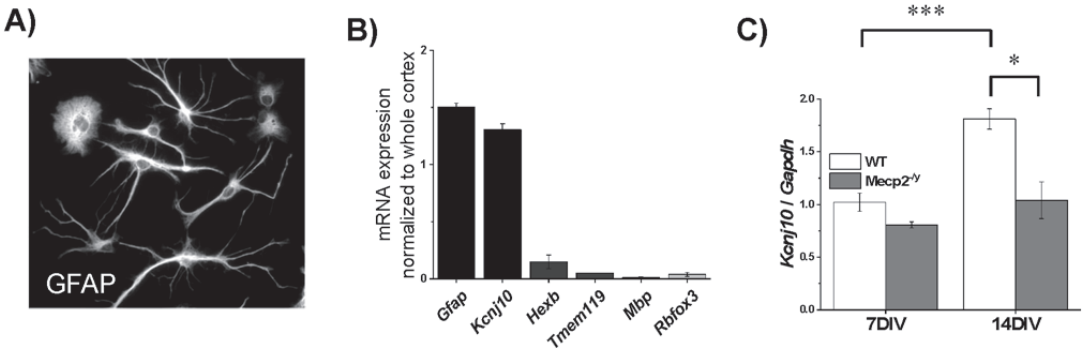

Figure 6

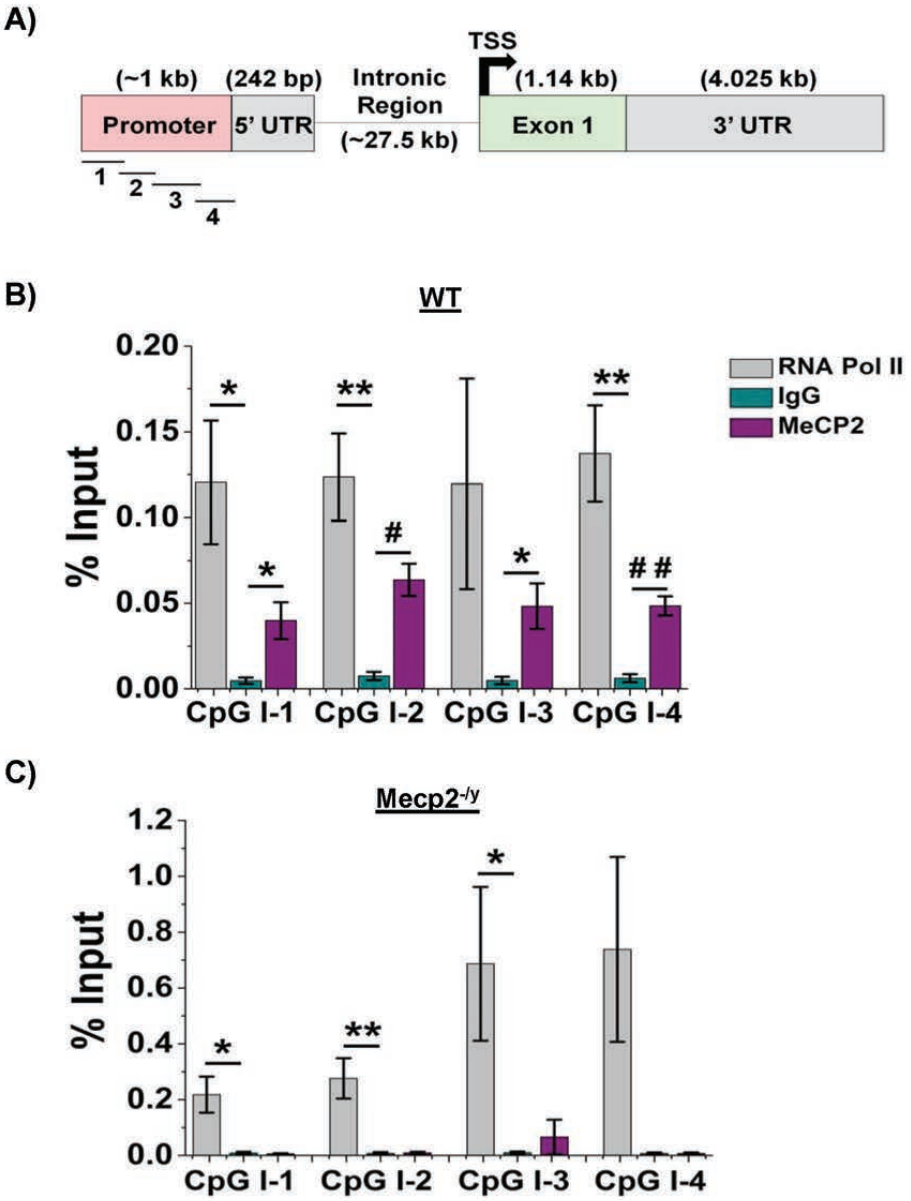

Figure 7

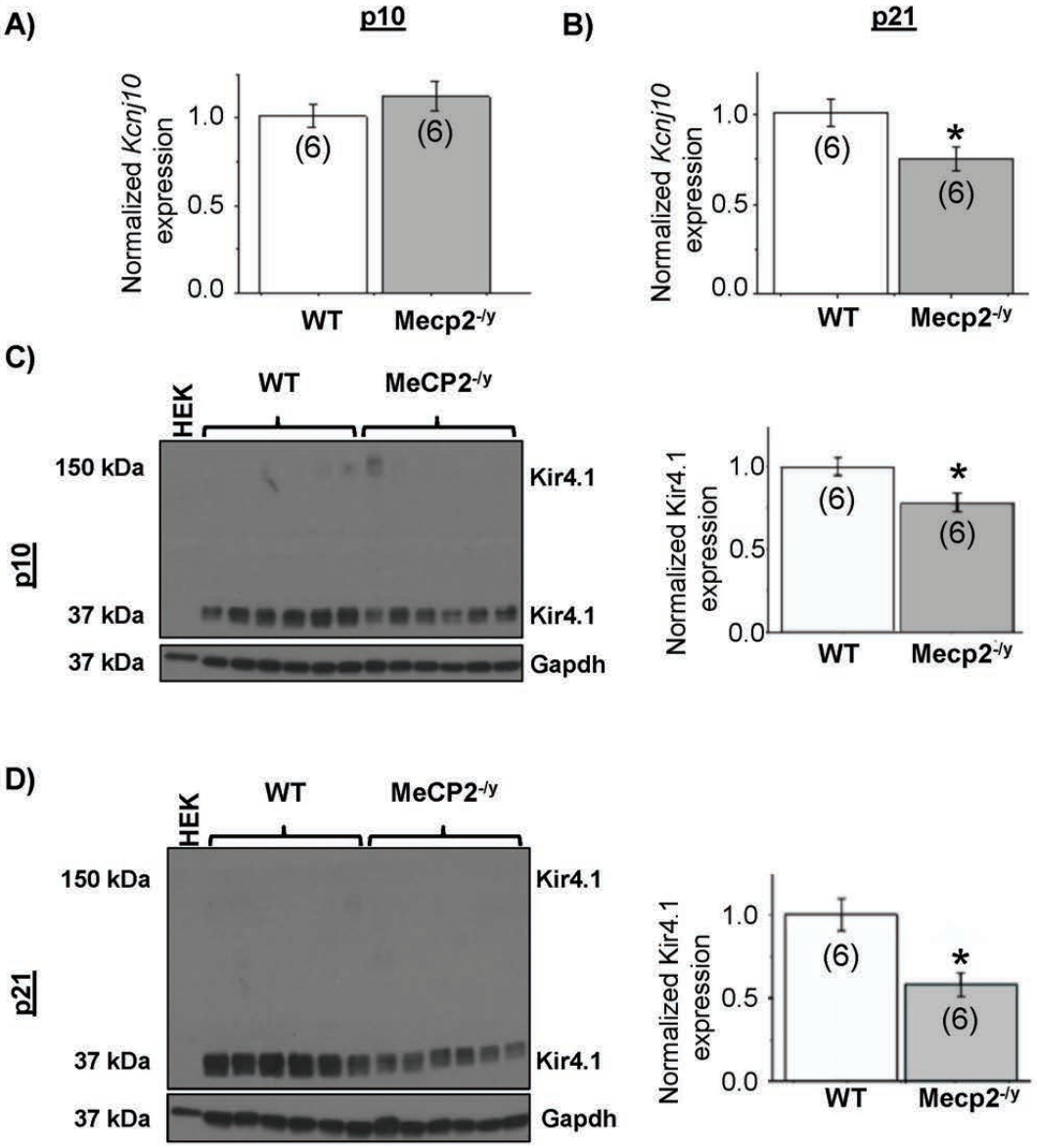

Table 1. Targeted Kir4.1 CpG Island I (promoter) PCR amplification sites

Target name	Forward Primer Sequences	Reverse Primer Sequences
CpG I-1	5'-AGTTTCCCTGCTTTCAATCCTG-3'	5'-CCTGTGGGAACACAGACACA-3'
CpG I-2	5'-GGATGGGAAGAGTTTGACGC-3'	5'-TACGGTGCAAAGTGTGGGAG-3'
CpG I-3	5'-CACACTTTGCACCGTACTGC-3'	5'-GATAGAAGCCGAGCTGGCAA-3'
CpG I-4	5'-GGCCGCCTCACTTTTCTTCT-3'	5'-TGGAGAGATTTGGGCAAGGC-3'

Table 2. RNA sequencing indicates of 14 *Kcnj* and 15 *Kcnk* potassium channels identified in the cortex of symptomatic MeCP2$^{-/y}$ mice and WT age matched littermates, only *Kcnj10*, *Kcnj16* and *Kcnk2* are differentially expressed (data mined from Pacheco et al., 2017).

Protein	**Gene Name**	**FPKM WT**	**FPKM TG**	**Fold Change**	**q value**	**Cell type specificity**
Kir4.1	Kcnj10	80.991	65.281	-0.311	0.00065	Astrocytes/oligodendrocytes/OPC's
Kir5.1	Kcnj16	14.832	11.353	-0.386	0.00853	Astrocytes/OPC's
TREK-1	Kcnk2	25.299	31.559	0.319	0.03503	Astrocytes/neurons/OPC's